



PCCP

**Time-Resolved Radiation Chemistry: Femtosecond Photoelectron Spectroscopy of Electron Attachment and Photodissociation Dynamics in Iodide-Nucleobase Clusters**

Journal:	<i>Physical Chemistry Chemical Physics</i>
Manuscript ID	CP-PER-12-2018-007831.R1
Article Type:	Perspective
Date Submitted by the Author:	07-Feb-2019
Complete List of Authors:	Kunin, Alice; University of California, Berkeley, Chemistry Neumark, Daniel; University of California, Dept of Chemistry

SCHOLARONE™  
Manuscripts

# **Time-Resolved Radiation Chemistry: Femtosecond Photoelectron Spectroscopy of Electron Attachment and Photodissociation Dynamics in Iodide-Nucleobase Clusters**

Alice Kunin<sup>1</sup> and Daniel M. Neumark<sup>1,2,\*</sup>

<sup>1</sup>*Department of Chemistry, University of California, Berkeley, California 94720, USA.*

<sup>2</sup>*Chemical Sciences Division, Lawrence Berkeley National Laboratory, Berkeley, California 94720, USA.*

\*Author to whom correspondence should be addressed: [dneumark@berkeley.edu](mailto:dneumark@berkeley.edu).

## **Abstract**

Iodide-nucleobase ( $I^- \cdot N$ ) clusters studied by time-resolved photoelectron spectroscopy (TRPES) are an opportune model system for examining radiative damage of DNA induced by low-energy electrons. By initiating charge transfer from iodide to the nucleobase and following the dynamics of the resulting transient negative ions (TNIs) with femtosecond time resolution, TRPES provides a novel window into the chemistry triggered by the attachment of low-energy electrons to nucleobases. In this Perspective, we examine and compare the dynamics of electron attachment, autodetachment, and photodissociation in a variety of  $I^- \cdot N$  clusters, including iodide-uracil ( $I^- \cdot U$ ), iodide-thymine ( $I^- \cdot T$ ), iodide-uracil-water ( $I^- \cdot U \cdot H_2O$ ), and iodide-adenine ( $I^- \cdot A$ ), to develop a more unified representation of our understanding of nucleobase TNIs. The experiments probe whether dipole-bound or valence-bound TNIs are formed initially and the subsequent time evolution of these species. We also provide an outlook for forthcoming applications of TRPES to larger iodide-containing complexes to enable the further investigation of microhydration dynamics in nucleobases, as well as electron attachment and photodissociation in more complex nucleic acid constituents.

## I. INTRODUCTION

DNA damage induced by low-energy electron attachment<sup>1</sup> has been a topic of considerable interest in recent years. Electron attachment to nucleobases and the subsequent formation of transient negative ions (TNIs) of the base has been implicated as the initial step in the damage mechanism.<sup>2-4</sup> It is predicted that single and double strand breaks then occur as a result of electron transfer from the base moiety to the sugar-phosphate backbone facilitated by strong electronic coupling.<sup>2, 3, 5, 6</sup> These considerations have motivated many experimental and theoretical studies of the interactions between nucleic acid constituents and low-energy electrons.<sup>7</sup>

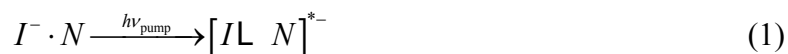
Nucleobases are capable of forming both a dipole-bound (DB) anion<sup>8</sup> in which the excess electron is trapped by the relatively large dipole moment of the base, or a conventional valence-bound (VB) anion<sup>3, 9</sup> by electron attachment to the  $\pi^*$  orbital of the base. Electron scattering experiments have suggested that the DB state is initially formed and may then convert or act as a “doorway” to the formation of a VB anion.<sup>10</sup> These metastable TNIs are then expected to decay, possibly leading to dissociation or fragmentation of the nucleobases, the larger nucleotide, or the DNA backbone structure.<sup>11, 12</sup> Many groups have studied the properties of these nucleobase DB and VB anions experimentally with a variety of techniques, including dissociative electron attachment<sup>10, 13-15</sup> and anion photoelectron spectroscopy.<sup>9, 16, 17</sup> Numerous theoretical studies of these anions have been carried out as well.<sup>18-22</sup> Of interest, however, is not only the electron binding properties and anionic dissociation channels but also the ultrafast time-resolved dynamics and evolution of these TNIs, including interconversion of a DB anion to form a VB anion, as well as the timescales for autodetachment, internal conversion, and fragmentation.

Our group has explored the time-resolved dynamics of electron attachment and transient decay in the nucleobase species uracil,<sup>23-26</sup> thymine,<sup>27</sup> and adenine,<sup>28</sup> as well as the uracil-water moiety,<sup>29</sup> using time-resolved photoelectron spectroscopy (TRPES) of iodide-nucleobase ( $I^- \cdot N$ ) clusters. We have measured and modelled the process of low-energy electron attachment to the nucleobase and observed the formation, evolution, and decay of both DB and VB anions for these  $I^- \cdot N$  clusters. In this Perspective, we provide an overview of these results for iodide-uracil ( $I^- \cdot U$ ), iodide-thymine ( $I^- \cdot T$ ), iodide-adenine ( $I^- \cdot A$ ), and iodide-uracil-water ( $I^- \cdot U \cdot H_2O$ ) clusters, and revisit the analyses of these studies based on the new insights provided by continued work on these clusters over the last five years. We also provide a framework for the continuation of these studies

and the application of this TRPES scheme to more complex iodide-containing biomolecule clusters.

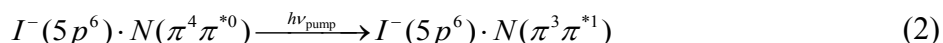
Anion photoelectron spectroscopy is an effective tool to probe DB and VB states since these anions are readily distinguished from one another by electron binding energy (eBE) as well as the shape of the photoelectron spectrum.<sup>16, 30</sup> DB anions are formed when an excess electron is bound by the dipole moment of a molecule, creating a weakly bound anion (typically <100 meV eBE) with the excess electron residing in a large, diffuse orbital outside of the molecular framework.<sup>8</sup> A molecular dipole moment of at least ~2-2.5 D is needed to bind the excess electron;<sup>31</sup> all of the canonical nucleobase species examined here have larger dipole moments than this and are thus capable of forming DB anions.<sup>32-34</sup> The neutral core of a DB state undergoes little or no geometry change upon photodetachment,<sup>35</sup> yielding a narrow peak in the anion photoelectron spectrum as there is negligible Franck-Condon activity. VB nucleobase anions, on the other hand, are conventional anions in which the excess electron resides in a valence orbital. For these species, the vertical detachment energy (VDE), corresponding to the difference in energy between the anion and the neutral at the equilibrium geometry of the anion, is typically hundreds of meV.<sup>9, 17, 36-39</sup> Moreover, the geometry of VB nucleobase anions is typically distorted relative to the neutral nucleobase in the ring puckering coordinate,<sup>18, 19, 27, 28, 40</sup> yielding a broad photoelectron spectrum.<sup>41</sup> Photoelectron spectra from Bowen and co-workers<sup>41</sup> (Fig. 1) for the U<sup>-</sup> DB anion and the U<sup>-</sup>·H<sub>2</sub>O VB anion exemplify the binding energy and spectral shape of these two types of negative ions.

This Perspective focuses on the application of TRPES to various I<sup>-</sup>·N clusters in order to probe the dynamics of electron attachment to nucleobases and the subsequent decay channels. The I<sup>-</sup>·N complexes have two regimes of UV photoabsorption:<sup>42</sup> the first is near-VDE photoexcitation corresponding to direct optical excitation by an ultraviolet (UV) pump pulse of energy  $h\nu_{\text{pump}}$  to initiate charge transfer from the iodide to the nucleobase moiety, labelled N in Eq. 1 below, creating a TNI.



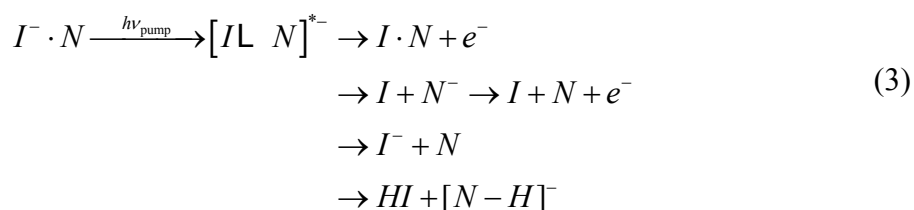
Excitations of this nature are clearly interesting as a model for reductive DNA damage by low-energy secondary electron attachment. The second regime of UV photoabsorption, measured to be

near 4.8 eV,<sup>42</sup> is calculated<sup>26, 42</sup> to encompass a strong base-centered  $\pi$ - $\pi^*$  excitation on the nucleobase with the excess electron still remaining with iodide, i.e.:



As discussed in more detail in Section IIIB, we believe this  $\pi$ - $\pi^*$  excitation is followed by rapid charge transfer from the iodide moiety to fill the hole in the  $\pi$  orbital of the base to create a VB anion. These higher energy excitations are also of interest in the DNA damage mechanism as the rapid, nonradiative photodeactivation pathways of  $\pi$ - $\pi^*$  UV photoexcited nucleobases are the core of the remarkable photostability of DNA.<sup>43-45</sup> Other optical transitions in  $I^- \cdot N$  clusters may also contribute to photoabsorption in this region; we explore the dynamics in this high energy photoexcitation regime for  $I^- \cdot U$  and  $I^- \cdot T$  clusters in detail in Section IIIB.

The time evolution of the TNI is traced by the probe pulse, which can photodetach the TNI or its photodissociation products at varying time delays. There are numerous energetically accessible decay pathways for the photoexcited  $I^- \cdot N$  clusters, including autodetachment, iodine loss,  $I^-$  formation, or a chemical reaction to form HI and a deprotonated nucleobase anion  $[N-H]^-$ , all of which are listed in Eq. 3.



While the 1.58 eV fundamental of Ti:Sapphire ultrafast lasers is sufficiently energetic as a probe to photodetach the nascent TNIs, higher energy UV probe pulses are required to photodetach many of the possible photofragments these complexes can form, including iodide (eBE = 3.059 eV)<sup>46</sup> and deprotonated nucleobase anions.<sup>47-49</sup>

In this Perspective, we begin in Section II with a discussion of the methodologies, both experimental and theoretical, used to understand the dynamics of these  $I^- \cdot N$  systems. In Section IIIA, we examine TRPES studies of the simpler, model system of photoexcited iodide-nitromethane ( $I^- \cdot \text{CH}_3\text{NO}_2$ ) clusters that provide an illustrative framework for understanding the

more complex dynamics of the larger nucleobase species. In Section IIIB, we delve into the dynamics of electron attachment and photodissociation in  $I^- \cdot U$  and  $I^- \cdot T$  clusters, which have been studied in more detail by TRPES as well as laser photodissociation spectroscopy. In particular, we cover results for  $I^- \cdot U$  and  $I^- \cdot T$  clusters following photoexcitation near the cluster VDE as well as photoexcitation in the higher energy regime near the base-centered  $\pi-\pi^*$  transition. In Section IIIC, we present recent results for electron attachment and photodissociation in photoexcited microhydrated  $I^- \cdot U \cdot H_2O$  clusters, and finally, in Section IIID we discuss TRPES studies of photoexcited  $I^- \cdot A$  clusters, which bear some similarities to  $I^- \cdot CH_3NO_2$  but pose additional challenges in analysis due to the propensity for tautomerization in gas phase adenine. We conclude with a summary of these systems and the salient information learned thus far as it relates to reductive damage of nucleic acid constituents and iodide-associated clusters in general. We also provide an outlook for the future avenues of this research and the application of TRPES of iodide-containing clusters to advance our understanding of reductive damage pathways in DNA.

## II. METHODOLOGIES

### A. Time-resolved photoelectron spectroscopy (TRPES)

A number of reviews dedicated to TRPES are available,<sup>50-62</sup> so we only briefly describe the key principles here as they relate to the study of TNIs. Single-photon anion photoelectron spectroscopy (PES), as shown schematically in Fig. 2a, involves the preparation of stable anions that can then be photodetached by an intersecting laser beam if the photon energy ( $h\nu$ ) exceeds the electron binding energy (eBE). The kinetic energy (eKE) distribution of the outgoing photodetached electrons is then measured, and the principle of energy conservation, as shown in Eq. 4, may then be used to determine accurate eBEs:

$$eBE = h\nu - eKE \quad (4)$$

Provided there is sufficient Franck-Condon overlap between the anion and neutral vibrational wavefunctions, photodetachment can occur to any neutral vibrational (and electronic) states within the photon energy range. In spectra that do not show any vibrational structure, the vertical detachment energy (VDE), or the difference in energy between the anion and the neutral at the equilibrium geometry of the anion, is identifiable as the peak or maximum intensity (maximum

Franck-Condon overlap) of the photoelectron spectrum, and the width of the spectrum is an indication of the geometry change that occurs upon photodetachment.

In the implementation of femtosecond (fs) anion TRPES used here, Fig. 2b, a fs pump pulse photoexcites a ground state  $I^- \cdot N$  anion to prepare an excited TNI, as in Eq. 1. A fs probe pulse then photodetaches the TNI to monitor, as a function of pump-probe delay, the ultrafast time evolution of the transient species. As described in the Introduction, a sufficiently energetic probe pulse can interrogate not only TNIs, but also any dissociation products that may form due to fragmentation of the evolving TNI. Thus, this technique effectively probes the ultrafast chemical dynamics of a TNI from formation through decay.

The experimental apparatus used for the TRPES studies herein, shown in Fig. 3, has been described in detail previously,<sup>63, 64</sup> and is briefly described here.  $I^- \cdot N$  clusters are generated by flowing 375-450 kPa of neon or argon buffer gas or 550 kPa of helium buffer gas over a reservoir of methyl iodide. This gas mixture is then passed into a pulsed Even-Lavie valve operating at 500 Hz that contains a cartridge with a solid sample of the nucleobase of interest heated to 205-220 °C. For the  $I^- \cdot CH_3NO_2$  studies, the cartridge is left empty; an additional reservoir on the gas line is filled with liquid  $CH_3NO_2$  and chilled in an ice water bath. For the  $I^- \cdot U \cdot H_2O$  studies, this reservoir is filled with deionized liquid water and heated, along with the connecting gas lines, to approximately 40 °C. In each configuration, the gas mixture is then supersonically expanded into vacuum through a ring filament ionizer to produce cluster anions. The anions are perpendicularly extracted into a Wiley McLaren time-of-flight mass spectrometer<sup>65</sup> and mass-selected to isolate the  $I^- \cdot N$  species of interest. These ions are photodetached through their interaction with one or two femtosecond laser pulses. The resultant photoelectrons are analyzed by velocity map imaging<sup>66</sup> on a chevron-stacked position-sensitive microchannel plate detector coupled to a phosphor screen and imaged using a charge-coupled device camera. Basis-set expansion (BASEX) reconstruction techniques<sup>67</sup> are used to reconstruct the 3D eKE distributions.

Various pump-probe schemes are employed among the studies in this work to excite and photodetach the  $I^- \cdot N$  clusters. A KMLabs Griffin oscillator and Dragon amplifier are used to generate 1.8-1.9 mJ/pulse laser pulses approximately 40-45 fs wide centered near 790 nm (1.57 eV) at a repetition rate of 1 kHz. Depending on the desired pump-probe scheme, these pulses are split into a pump arm and a probe arm delayed by a delay stage. In the pump arm, UV light is usually generated by frequency-doubling the output of a LightCon TOPAS-C optical parametric

amplifier with a  $\beta$ -barium borate (BBO) crystal. This scheme yields pump pulses between 235 nm - 350 nm of approximately 8-13  $\mu\text{J}/\text{pulse}$ . The fundamental infrared (IR) of the KMLabs system can be used as the probe beam (1.57 eV, 80  $\mu\text{J}/\text{pulse}$ ), or the fundamental can be frequency-doubled in a BBO crystal to yield 395 nm pulses (3.14 eV, 65  $\mu\text{J}/\text{pulse}$ ). Other schemes include recovering the residual fundamental from the TOPAS-C to use as the probe, or recovering residual visible non-frequency-doubled TOPAS-C output to recombine nonlinearly in a BBO crystal with the fundamental pulse to yield UV probe pulses in the range of 340-360 nm ( $\sim 10$   $\mu\text{J}/\text{pulse}$ ). We refer the reader to the individual  $\text{I}^- \cdot \text{N}$  papers referenced herein for the specific laser scheme details for each study. The cross-correlation measured at the vacuum chamber for the pump and probe laser pulses is typically  $\sim 150$ -185 fs for UV/IR-type pump/probe schemes and  $\sim 200$ -220 fs for UV/UV-type pump/probe schemes.

## B. Computational methods

We comment briefly on the various computational methods used to characterize both the ground states and the excited states of  $\text{I}^- \cdot \text{N}$  anionic clusters, as these calculations can greatly inform the analysis and interpretation of the measured experimental results. The detailed work described herein was performed using the Gaussian 03 or Gaussian 09 computing packages.<sup>68, 69</sup> The results of these theoretical methods applied to specific  $\text{I}^- \cdot \text{N}$  clusters are described further in the corresponding sections that follow.

Theoretical work on the interaction of iodide with a uracil molecule was first performed by Ortiz and co-workers,<sup>70</sup> who employed second-order Møller-Plesset theory (MP2) with augmented, correlation-consistent triple- $\zeta$  (aug-cc-pVTZ) bases<sup>71</sup> and an augmented Stuttgart pseudopotential (-pp)<sup>72</sup> to calculate the VDE of the  $\text{I}^- \cdot \text{U}$  cluster. These calculations found the  $\text{I}^- \cdot \text{U}$  cluster VDE to be approximately 4.16 eV, and the cluster structure to be planar with the charge localized on the iodine atom. Since then, Takayanagi and co-workers have employed various density functional theory (DFT) functionals and diffuse basis sets as well as long-range corrected (LC)-DFT to examine several species of interest including anionic uracil, uracil-water, thymine, and adenine, as well as  $\text{I}^- \cdot \text{U}$ , and  $\text{I}^- \cdot \text{T}$ .<sup>19-21, 27, 28</sup> Their calculations have focused on the use of these methods to determine the structure and energetics of these species, the DB to VB anion conversion barrier height and transition state geometry, and simulations of photoelectron spectra.



Our group has carried out calculations at the MP2/aug-cc-pVDZ(-pp) level of theory as well as the coupled cluster singles and doubles (CCSD)/aug-cc-pVDZ(-pp) level of theory to calculate anion ground state structures and VDEs for each of the  $I^- \cdot N$  cluster systems examined here to inform our experimental measurements.<sup>23, 24, 26-29, 73</sup> Table I presents the structure for each ground state anion, as well as the dipole moment of the neutral  $I \cdot N$  species at the equilibrium geometry of the anion. In all cases, the  $I^-$  binds primarily to the most acidic H atom on the nucleobase. The VDEs of the  $I^- \cdot N$  species reported in Table 1 are those experimentally measured by single-photon PES.

Takayanagi et al.<sup>27</sup> have performed excited state calculations at the time-dependent (TD)-DFT/ $\omega$ B97XD/aug-cc-pVDZ(-pp) level of theory for  $I^- \cdot U$  and  $I^- \cdot T$ , and Dessent et al.<sup>42</sup> at the TD-DFT/B3LYP/6-311++G(2d,2p) and 6-311G(d,p)(-pp) level of theory<sup>74-79</sup> for  $I^- \cdot U$ ,  $I^- \cdot T$ , and iodide-cytosine ( $I^- \cdot C$ ). These excited state calculations are valuable for the analysis of the  $I^- \cdot N$  cluster absorption profiles as they elucidate the energetics and character of the various possible transition channels. Our group<sup>26, 29</sup> has performed equation-of-motion (EOM)-CCSD calculations based on  $I^- \cdot U$  and  $I^- \cdot U \cdot H_2O$  structures optimized at the MP2/aug-cc-pVDZ(-pp) level of theory. Although computationally expensive, these wavefunction-based calculations have proved effective at identifying the DB state for both of these species and are expected to provide among the best possible theoretical results for the nature of the initially formed photoexcited charge transfer states in our TRPES experiments.

One of the decay mechanisms for photoexcited  $I^- \cdot N$  clusters is internal conversion followed by fragmentation to  $I^- + N$ . To analyze this photodissociation mechanism further, our group has also performed Rice-Ramsperger-Kassel-Marcus (RRKM) calculations to estimate the rate of statistical unimolecular dissociation for these photoexcited species to yield  $I^-$ .<sup>26, 80</sup> Variational transition state theory was used to determine the transition state along the barrierless iodide-molecule stretching coordinate potential energy curve. The zero-point energy corrected energy difference between the ground and transition state was then used to calculate the microcanonical reaction rate constant using the Beyer-Swinehart algorithm<sup>81</sup> to calculate the reactant density of states and transition state sum of states. The Stein-Rabinovitch modification<sup>82</sup> was used to treat low-energy iodide-molecule  $I^- \cdots M$  in-plane and out-of-plane modes as hindered internal rotors.

### III. Electron Attachment and Photodissociation in $I^- \cdot N$ Clusters

In order to emphasize trends across the range of systems studied here, one-photon and TRPE spectra for each  $I^- \cdot N$  species are shown in Figs. 4-7. Figs. 4a)-e) show one-photon photoelectron spectra for  $I^- \cdot CH_3NO_2$ ,  $I^- \cdot U$ ,  $I^- \cdot T$ ,  $I^- \cdot U \cdot H_2O$ , and  $I^- \cdot A$ , respectively. Figs. 5a)-e) show near-VDE photoexcited TRPE spectra for the same five systems along with the time-evolution of TNI production and decay at both early and long delay times. Figs. 6a)-d) show the time-evolution of  $I^-$  production via photodissociation for select systems and excitation energies, and Figs. 7a) and b) show the TRPE spectra and time-dependent signal evolution for  $I^- \cdot U$  and  $I^- \cdot T$  photoexcited at excitation energies near  $\sim 4.7$  eV. These results are considered in more detail in the subsections below. For consistency and ease of comparison throughout this work, we refer to the TRPES pump energies employed here relative to the cluster VDE by  $h\nu_{pump} - VDE$ .

#### A. $I^- \cdot CH_3NO_2$

We begin by first considering the photoexcited  $I^- \cdot CH_3NO_2$  binary complex, which serves as an interesting model system for conversion between DB and VB anions. Nitromethane ( $CH_3NO_2$ ) has a sufficiently large dipole moment, 3.46 D, to bind an electron in a DB state and also supports a conventional valence bound anion, which lies lower in energy and is the ground state of the anion.<sup>30, 83, 84</sup> Both DB and VB anions of  $CH_3NO_2^-$  have been measured by photoelectron spectroscopy; the DB anion has a VDE of  $8 \pm 8$  meV, and the VDE of the VB anion is 0.9-1 eV.<sup>30, 85</sup>

$I^- \cdot CH_3NO_2$  binary complexes have been studied with photofragment action spectroscopy by Dessent and Johnson.<sup>83</sup> This work has identified the  $I^- \cdot CH_3NO_2$  cluster VDE as  $3.60 \pm 0.01$  eV and detected evidence for the presence of the  $I^- \cdot CH_3NO_2$  DB anion. Our group has performed two sets of TRPES studies of  $I^- \cdot CH_3NO_2$  clusters photoexcited near the cluster VDE with two aims: 1.56 eV probe experiments to test for the presence of DB and VB anions of nitromethane,<sup>73</sup> and 3.14 eV probe experiments to measure the time-resolved formation of  $I^-$  and other photofragments.<sup>80</sup>

The single-photon photoelectron spectrum of  $I^- \cdot CH_3NO_2$  is shown in Fig. 4a. Feature A, the lowest energy and most intense feature, and the location of its maximum, 3.60 eV, should be the cluster VDE; this value matches previous experimental results for  $I^- \cdot CH_3NO_2$ .<sup>83</sup> Feature A corresponds to detachment to the lower spin orbit state of the complex  $I(^2P_{3/2}) \cdot CH_3NO_2$ , while

feature B, appearing near 4.5 eV, corresponds to photodetachment to the upper spin orbit state of the complex  $I(^2P_{1/2})\cdot\text{CH}_3\text{NO}_2$ , lying approximately 0.94 eV higher in energy.<sup>86</sup>

In the first set of time-resolved experiments,  $I^-\cdot\text{CH}_3\text{NO}_2$  clusters are photoexcited at the VDE and probed at 1.56 eV.<sup>73</sup> Fig. 5a shows the TRPE spectra for  $I^-\cdot\text{CH}_3\text{NO}_2$  photoexcited at 3.60 eV. The left panel shows a false-color two-dimensional plot of eBE versus pump-probe delay. There is a narrow, short lived feature (A) with a low eBE that is assigned to a DB state, and a broader, longer lived feature (B) assigned to a VB state. The center and right panels of Fig. 5a show integrated intensities of feature A (blue) and feature B (red) at short and longer time delays, respectively. A similar layout is used for the other rows of Fig. 5.

The nascent  $[I\cdots\text{CH}_3\text{NO}_2]^-$  DB anion appears within the cross-correlation of the pump and probe laser pulses,  $<150$  fs. The DB anion decays mono-exponentially in  $460 \pm 60$  fs, while the  $[I\cdots\text{CH}_3\text{NO}_2]^-$  VB anion appears in  $420 \pm 50$  fs. This close match-up in lifetimes indicates that the DB anion decays primarily to form the VB anion in a rapid and complete or nearly-complete conversion. The VB state was measured to decay bi-exponentially with time constants of 2 ps and 1300 ps.

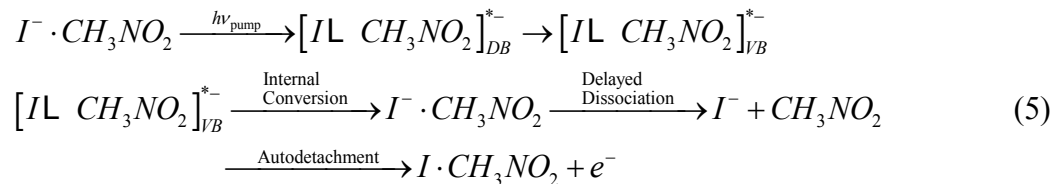
Photoelectron signal corresponding to autodetachment was also measured as near  $\sim 0$  eV eKE signal from photoexcited  $I^-\cdot\text{CH}_3\text{NO}_2$  clusters.<sup>73</sup> Autodetachment refers to the spontaneous ejection of an electron following photoexcitation of an anion resonance. If a nascent metastable photoexcited anion lies isoenergetically within a manifold of vibrational levels of the corresponding neutral plus a free electron, then nonadiabatic coupling between the electronic and nuclear degrees of freedom can facilitate the detachment of an electron.<sup>35, 87, 88</sup> In the specific case in which the internal energy of the excited anion (or cluster) is randomized prior to electron ejection, the detached electron typically carries  $\sim 0$  eV electron kinetic energy (eKE) and this statistical process is referred to as thermionic emission.<sup>89, 90</sup> Since the DB state appears to decay solely to the VB anion, it is reasonable to attribute at least one of the biexponential decay constants of the VB anion to autodetachment.

To further characterize the decay dynamics of the  $[I\cdots\text{CH}_3\text{NO}_2]^-$  VB anion, a second experiment with 3.56 eV pump energy ( $-40$  meV) and 3.14 eV probe energy was performed.<sup>80</sup> This pump-probe scheme enables detection of photodissociation channels that yield  $I^-$  (eBE = 3.059 eV)<sup>46</sup> or the nitromethide anion  $\text{CH}_2\text{NO}_2^-$  (VDE =  $2.635 \pm 0.010$  eV),<sup>80, 91</sup> both of which can be photodetached with the higher energy 3.14 eV probe pulse.  $I^-$  was measured as the major

photofragmentation channel with a mono-exponential rise time of  $21 \pm 1$  ps, shown in Fig. 6a. This finding suggests that the shorter time constant for VB anion decay (2 ps) corresponds to back-electron transfer to re-form  $\text{I}^- \cdot \text{CH}_3\text{NO}_2$ , followed by internal conversion (IC) to the  $\text{I}^- \cdot \text{CH}_3\text{NO}_2$  anion ground state and, finally, dissociation to yield  $\text{I}^-$ .

Given the relatively long  $\text{I}^-$  rise time compared to the approximately 2 ps short decay time of the  $[\text{I} \cdots \text{CH}_3\text{NO}_2]^-$  VB anion, RRKM calculations were performed to analyze the statistical dissociation of  $\text{I}^- \cdot \text{CH}_3\text{NO}_2$  complexes to yield  $\text{I}^-$ .<sup>80</sup> These RRKM calculations yielded dissociation rates of approximately 300-400 fs, depending on the treatment of internal rotations in the  $\text{I}^- \cdot \text{CH}_3\text{NO}_2$  complex. This calculated lifetime is quite fast and is unlikely to be a realistic physical timescale for intramolecular vibrational energy redistribution (IVR) and subsequent dissociation in a cluster, and indicates that there exists some dynamical bottleneck in the formation of  $\text{I}^-$  from  $\text{I}^- \cdot \text{CH}_3\text{NO}_2$ .

The  $[\text{I} \cdots \text{CH}_3\text{NO}_2]^-$  DB anion is expected to geometrically resemble the neutral iodine-nitromethane species as the electron resides largely outside the molecular framework, while the  $[\text{I} \cdots \text{CH}_3\text{NO}_2]^-$  VB anion is expected to more closely resemble the puckered  $\text{CH}_3\text{NO}_2^-$  geometry in which the  $-\text{NO}_2$  is out of the plane of the molecule.<sup>73, 85</sup> During the DB to VB anion transition, it can therefore be expected that the  $-\text{NO}_2$  vibrational modes become vibrationally excited as the VB anion is formed. We therefore suggest that a dynamical bottleneck arises in  $\text{I}^- \cdot \text{CH}_3\text{NO}_2$  from inefficient energy flow from these high frequency  $-\text{NO}_2$  vibrational modes to the relatively low frequency ( $<100 \text{ cm}^{-1}$ )  $\text{I} \cdots \text{CH}_3\text{NO}_2$  modes that will ultimately yield  $\text{I}^-$  dissociation. Hase and co-workers<sup>92, 93</sup> and Brauman and co-workers<sup>94</sup> have theoretically examined a number of  $\text{X}^- + \text{CH}_3\text{Y} \rightarrow \text{CH}_3\text{X} + \text{Y}^-$  gas phase  $\text{S}_{\text{N}}2$  reactions for X and Y as halogens or molecular species and have shown that energy transfer between high energy and low energy vibrational modes may be inefficient and lead to non-statistical dynamics.<sup>95, 96</sup> Thus, IVR within the  $\text{I}^- \cdot \text{CH}_3\text{NO}_2$  complex reformed from the VB anion can act as the rate-limiting step in the dissociation of these complexes. We therefore conclude that the fast bi-exponential decay of the VB anion is IC to the ground state followed by delayed  $\text{I}^-$  evaporation, and the long-time VB anion decay (1300 ps) is by autodetachment. The proposed scheme for the photoinduced dynamics of  $\text{I}^- \cdot \text{CH}_3\text{NO}_2$  are summarized by Eq. 5:



The rapid and complete DB anion to VB anion conversion following near-VDE photoexcitation of  $I^- \cdot CH_3NO_2$ , in addition to the observed non-statistical decay to yield  $I^-$ , provides insight into the energetics of the TNI partial conversion process and also the possible interactions between the iodine atom and the  $CH_3NO_2$  moiety. We take these observed  $I^- \cdot CH_3NO_2$  dynamics into consideration to help inform the studies of the  $I^- \cdot N$  clusters in the discussion that follows.

### B. $I^- \cdot$ Uracil and $I^- \cdot$ Thymine Binary Complexes

The pyrimidine bases uracil and thymine both have dipole moments of approximately 4.15 D, so each can support a DB anion.<sup>34</sup> Photoelectron spectroscopy has previously found both the uracil and thymine DB anions to have eBEs of approximately 90 meV and 70 meV, respectively.<sup>16</sup> No photoelectron spectrum has been recorded for the VB anion of either uracil or thymine, but Rydberg electron transfer experiments<sup>37</sup> as well as theoretical calculations<sup>36, 97</sup> predict that both the DB anion as well as the VB anion for both nucleobases exist, at least as TNIs, with VB anion VDEs of approximately 500 meV. For both uracil and thymine, the DB anion is the anionic ground state,<sup>41, 98</sup> with a predicted barrier of 36-155 meV for conversion to form the VB anion, depending on the level of theory.<sup>27</sup> However, bare thymine has been calculated to have a ~10-20 meV higher conversion barrier for DB to VB anion conversion than bare uracil at each calculation method and basis set combination employed.<sup>27</sup>

The time-resolved dynamics of  $I^- \cdot U$  and  $I^- \cdot T$  clusters have been explored at photoexcitation energies near the VDE<sup>25, 27</sup> as well as in the higher energy (~4.6-4.9 eV) excitation regime.<sup>23, 24, 26</sup> Laser photodissociation spectroscopy experiments by the Dessent group, in combination with theoretical results, complement the analysis of the time-resolved work described in more detail here.<sup>26, 42</sup> In this section, we consider the dynamics for  $I^- \cdot U$  and  $I^- \cdot T$  in these two photoexcitation regions both at early delay times to examine the dynamics of TNI formation and at longer delay times to probe the various autodetachment and dissociation channels.

One-photon photoelectron spectra at multiple photon energies are reproduced for  $I^- \cdot U$  and  $I^- \cdot T$  in Fig. 4b and 4c, respectively. Feature A corresponds to direct detachment to the  $I(^2P_{3/2}) \cdot N$  neutral complex, yielding VDEs of  $4.11 \pm 0.05$  eV<sup>23, 24</sup> and  $4.05$  eV  $\pm 0.05$  eV<sup>24</sup> for  $I^- \cdot U$  and  $I^- \cdot T$ , respectively. Feature B, seen only at the highest photon energies, arises from photodetachment to the upper iodine spin-orbit state. Feature C, which corresponds to  $\sim 0$  eV eKE photoelectron signal from autodetachment, is also present at each detachment energy. Two interesting trends can be seen in this autodetachment signal. At all photon energies, there is somewhat stronger autodetachment signal from  $I^- \cdot T$  than  $I^- \cdot U$  relative to peak A, the direct detachment feature. Moreover, the intensity of the autodetachment signal appears to reach a maximum near 4.7-4.8 eV photon energy, and declines at energies above and below this region. We explore these trends and the origin of the autodetachment signal in more detail below with the assistance of laser photodissociation spectroscopy, excited state calculations, and the time-resolved results.

Laser photodissociation spectroscopy has been carried out on  $I^- \cdot U$  and  $I^- \cdot T$  by Dessent et al;<sup>26, 42</sup> the photodepletion (photoabsorption, including dissociation and detachment) profiles for  $I^- \cdot U$  and  $I^- \cdot T$  from 3.6 to 5.3 eV are reproduced here in Fig. 8a and 8b, respectively (black dots, with the red lines indicating five-point adjacent averages). Two regimes of UV photoabsorption are measured: the first excited state in the vicinity of the VDE, centered at approximately 4 eV for both clusters, and the second centered around 4.8 eV. The photofragment yields of  $I^-$  for  $I^- \cdot U$  and  $I^- \cdot T$  are shown in Figs. 8c and 8d, respectively.  $I^-$  and  $[N-H]^-$ , the deprotonated nucleobase anion, were measured as the photofragments for both clusters, with  $I^-$  appearing as the overwhelmingly dominant species.<sup>42</sup> Both photofragments form in two distinct bands of photoexcitation: one centered near the VDE of each cluster, and one centered near 4.8 eV.

For ease of comparison of results, in Fig. 8 we overlay these laser photodissociation results with the respective  $I^- \cdot U$  and  $I^- \cdot T$  one color photoelectron spectra from Figs. 4b and 4c. The near-VDE photoabsorption and photofragmentation bands appear at lower energies than the VDE photodetachment bands; this has been observed previously and is due to the fact that photodetachment is not possible below the VDE, but photoabsorption and formation of the DB anion is possible and has been measured at pump energies below the VDE, as described in more detail in this section.<sup>25-27, 42</sup> More interestingly, the autodetachment feature present in the one color spectra for both  $I^- \cdot U$  and  $I^- \cdot T$  appears to track closely with the higher energy photoabsorption and

$\Gamma^-$  photofragmentation bands; we consider this finding and the dynamics resulting from high energy photoexcitation in more detail in Section IIIB.

Excited state calculations have been performed at the TD-DFT/B3LYP level for  $\Gamma^- \cdot U$  and  $\Gamma^- \cdot T$ ,<sup>42</sup> and at the EOM-CCSD/aug-cc-pVDZ(-pp) level for  $\Gamma^- \cdot U$ <sup>26</sup> to examine the nature of photoexcitation in each of the two energy regimes in more detail. The EOM-CCSD results find three transitions with prominent oscillator strength in the energy region near the VDE corresponding to excitation from an iodide ( $5p$ ) orbital to form a DB state of the complex (Fig. 8e). By far, the strongest transition near 4.8 eV was calculated to be a base-centered  $\pi-\pi^*$  excitation (Fig. 8f), with two less intense channels (approximately 10x less oscillator strength) near 4.7 eV corresponding to excitation from an iodide ( $5p$ ) orbital to a  $\sigma^*$  state of the complex (Fig. 8g). The TD-DFT calculations for both  $\Gamma^- \cdot U$  and  $\Gamma^- \cdot T$  also find base centered  $\pi-\pi^*$  excitation to be the most prominent excitation channel, with four less intense  $I(5p) \rightarrow \sigma^*$  transitions in  $\Gamma^- \cdot U$  in the energy region near the  $\pi-\pi^*$  excitation, and two such transitions in  $\Gamma^- \cdot T$  (2-3x less oscillator strength in  $\Gamma^- \cdot U$ , 3-18x less in  $\Gamma^- \cdot T$ ). No evidence is found in either set of excited state calculations for channels with significant oscillator strength corresponding to  $I(5p) \rightarrow \pi^*$  charge transfer, i.e. direct optical excitation to form the VB anion, presumably reflecting near-zero spatial overlap between these initial and final states. Thus, we may expect that photoexcitation near the VDE most likely yields direct optical excitation from iodide to form the DB anion instantaneously, while photoexcitation at higher pump energies will most likely yield dynamics with the largest contribution from base-centered  $\pi-\pi^*$  excitation, although  $I(5p) \rightarrow \sigma^*$  type charge transfer may also be active to a lesser extent. We now turn our attention to the time-resolved results of photoexcitation of  $\Gamma^- \cdot U$  and  $\Gamma^- \cdot T$  clusters in each of these two pump energy regimes.

### 1. Early time dynamics from near-VDE excitation of $\Gamma^- \cdot U$ and $\Gamma^- \cdot T$

TRPES studies of  $\Gamma^- \cdot U$  clusters were carried out at pump excitation energies from -110 meV to +100 meV relative to the VDE,<sup>25</sup> and are shown at +30 meV in Fig. 5b. At each of these excitation energies, both the DB anion (feature A, blue) and the VB anion (feature B, red) of  $\Gamma^- \cdot U$  were observed. The DB anion rise time decreases from approximately 250 fs to  $\leq 150$  fs as the pump energy is increased from -110 meV to +100 meV, while the VB anion rise time remains near 250 fs over this pump energy range.

The TRPES studies of  $I^- \cdot T$  employed pump energies ranging from -120 meV to +90 meV in an analogous fashion to the  $I^- \cdot U$  studies, and are shown for +20 meV in Fig. 5c. Both the DB anion and the VB anion of  $I^- \cdot T$  were observed each at pump energy. The DB anion appears in approximately 230 fs, exhibiting no dependence on the pump excitation energy. The VB anion forms in approximately 300 fs, with clear energy dependence only revealed at the lowest pump energy used, -120 meV, which yielded a VB anion rise time over 1 ps.

The findings for  $I^- \cdot U$  and  $I^- \cdot T$  that the DB rise time is faster or the same as that for the VB anion indicate that the DB state is formed first, followed by appearance of VB signal. The calculations in Section IIIB show that there is no direct excitation of the VB state near the VDE, so we propose that the DB anion is created by photoexcitation and the VB signal results from DB to VB anion conversion. However, the observation that the DB signal remains while the VB signal grows in suggests that at most only partial DB to VB anion conversion occurs subsequent to photoexcitation. In contrast to  $I^- \cdot CH_3NO_2$ , the DB anion is the anionic ground state for uracil and thymine,<sup>41, 98</sup> and the barrier for conversion to form the VB anion is calculated to lie approximately ~36-155 meV higher in energy,<sup>18, 20, 21, 27</sup> depending on the level of theory. As a result, it is reasonable that the dynamics of DB to VB anion conversion differ from the complete conversion in  $I^- \cdot CH_3NO_2$ .

Note that while the  $I^- \cdot CH_3NO_2$  TRPE spectrum shows a cross-correlation limited rise time for the DB anion, the  $I^- \cdot U$  and  $I^- \cdot T$  DB anions (and those of other  $I^- \cdot N$  clusters presented here) exhibit finite rise times. This rise time may originate from an increase in the photodetachment cross section as a result of iodine-nucleobase motion following the vertical formation of the TNI.<sup>27</sup> The DB orbital calculated for  $I^- \cdot U$  in Fig. 8e appears to avoid the iodine atom; iodine is calculated to sit within the region where the DB orbital for bare uracil has been calculated to exist.<sup>22</sup> We have previously proposed that following initial photoexcitation, the iodine atom moves in such a way as to decrease the repulsive interaction between the diffuse DB orbital and the iodine atom.<sup>25, 27</sup> This increased localization of the DB orbital is expected to increase the photodetachment cross section for the DB anion at early times, manifesting in a finite rise time for the DB anion.<sup>27</sup>

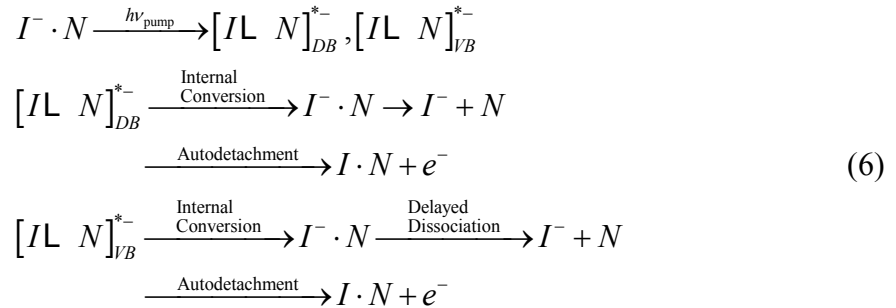
## 2. Long time dynamics of near-VDE excited $I^- \cdot U$ and $I^- \cdot T$ clusters

The DB and VB TNI signals for  $I^- \cdot U$  and  $I^- \cdot T$  clusters decay bi-exponentially, with each set of lifetimes generally decreasing with increasing pump excitation energy in the near-VDE



regime. For  $I^- \cdot U$  photoexcited at +30 meV (Fig. 5b), the DB anion bi-exponential decay constants are 5.0 ps and 500 ps, while the VB anion undergoes bi-exponential decay in 5.6 ps and 80 ps.<sup>25</sup>  $I^- \cdot T$  photoexcited at +20 meV (Fig. 5c) similarly exhibits DB anion decay in 5.2 ps and 1100 ps, and VB anion decay in 13.1 ps and 530 ps.<sup>27</sup>

Two decay pathways have been measured in our TRPES work on near-VDE photoexcited  $I^- \cdot U$  clusters: autodetachment and bi-exponential re-formation of  $I^-$ . Autodetachment has been measured in TRPES of  $I^- \cdot U$  and  $I^- \cdot T$  at all near-VDE photoexcitation energies as near 0 eV eKE signal with initial depletion dynamics followed by intensity recovery at longer times, although the dynamics for ~0 eV signal are challenging to extract here with certainty. TRPES of  $I^- \cdot U$  clusters photoexcited at 4.03 eV (-80 meV) and probed at 3.61 eV finds bi-exponential formation of  $I^-$  in  $17.5 \pm 1.6$  ps and  $150 \pm 10$  ps as the only major photodissociation pathway; this  $I^-$  rise signal is shown in Fig. 6b, and is attributed to internal conversion followed by fragmentation. The overall decay mechanisms for the DB and VB anions are given by Eq. 6.



To assign the bi-exponential  $I^-$  rise dynamics in near-VDE photoexcited  $I^- \cdot U$ , we compare the dynamics here to the mechanism of  $I^-$  reformation in  $I^- \cdot CH_3NO_2$ . There, we observed complete DB to VB anion conversion and concluded that the fast decay component of the VB anion may be decay by IC to the  $I^- \cdot CH_3NO_2$  ground state followed by dissociation to yield  $I^-$  at a delay due to a dynamical bottleneck. Thus, for  $I^- \cdot U$  clusters we may expect, since both TNIs are present as the DB to VB anion conversion is only partially complete, that each TNI has a fast decay process of IC to the electronic  $I^- \cdot U$  ground state followed by evaporation of  $I^-$  to ultimately yield bi-exponential  $I^-$  rise rather than the solely mono-exponential rise observed in  $I^- \cdot CH_3NO_2$  clusters. Given that the fast  $I^-$  rise time of 17.5 ps from  $I^- \cdot U$  is a few ps longer than both the DB anion and VB anion fast decay lifetimes, it is possible for  $I^- \cdot U$  clusters that the fast  $I^-$  appearance arises from

IC of the DB anion, and the slow  $I^-$  appearance of 150 ps originates from IC and delayed ejection of  $I^-$  from the VB anion.

We expect that the long time decays of each TNI for both species are from autodetachment, or rather, more specifically, by thermionic emission considering the  $\sim 100$  ps – 1 ns long decay lifetimes of each TNI. Such a statistical mechanism is congruent with the decrease in the long time constants with increasing pump energy as measured here. The DB anion of  $I^- \cdot U$  clusters, for example, exhibits a decrease in the long time constant from 2000 ps to 30 ps in the range of pump excitation from -110 meV to +100 meV.<sup>25</sup> Laser photodissociation spectra find  $[U-H]^-$  (neutral electron affinity = 3.481 eV)<sup>47</sup> as an additional minor dissociation product from  $I^- \cdot U$  clusters, but due to its minor abundance and molecular cross section, we did not observe this channel in our TRPES studies.

### 3. Dynamics of $I^- \cdot U$ and $I^- \cdot T$ excited at higher energy

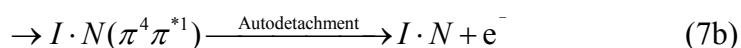
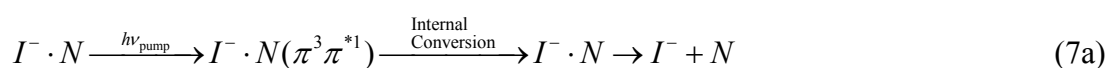
TRPES studies for  $I^- \cdot U$  and  $I^- \cdot T$  were also conducted at pump excitation energies from 4.6 eV – 4.9 eV.<sup>23, 24</sup> TRPE spectra for  $I^- \cdot U$  and  $I^- \cdot T$  photoexcited at 4.69 eV and probed at 1.57 eV are shown in Figs. 7a and 7b, respectively. In this energy regime, no evidence for the existence of a DB state was measured for either cluster. Both species exhibit VB anion signal (red integrated intensity) with a cross-correlation limited rise ( $\leq 150$  fs), as well as time-dependent signal at  $\sim 0$ -0.08 eV eKE corresponding to autodetachment (black integrated intensity). At this excitation energy, the  $I^- \cdot U$  VB anion decays bi-exponentially in 620 fs and 52 ps, while the  $I^- \cdot T$  VB anion undergoes mono-exponential decay<sup>27</sup> in  $\sim 610$  fs. The lifetimes for the  $I^- \cdot U$  VB anion bi-exponential decay were found to decrease somewhat with increasing pump energy, while the  $I^- \cdot T$  VB anion mono-exponential decay did not exhibit excitation energy dependence in this high energy pump regime. The autodetachment signal for both clusters was measured to exhibit non-zero autodetachment intensity at negative times, prompt depletion at  $t=0$  fs, and recovery to the initial intensity, although the signal in  $I^- \cdot U$  clusters was found to exceed its initial intensity. As seen in the integrated intensities in Fig. 7b, in  $I^- \cdot T$  clusters, the VB anion prompt appearance and decay time constant mirrors the time constants for the autodetachment dynamics.<sup>24</sup>

TRPES of  $I^- \cdot U$  at 4.72 eV pump energy with 3.15 eV probe energy finds mono-exponential appearance of  $I^-$  in  $36 \pm 3$  ps as the major photodissociation channel (Fig. 6c), as well as TRPES signal arising from autodetachment. The 3.15 eV probe study also measured autodetachment

depletion and recovery but without any long-time overshoot of the initial intensity, although these dynamics are noisier due to the very close energetic overlap of the  $\sim 0.08$  eV eKE autodetachment signal with  $I^-$  photodetachment ( $\sim 0.09$  eV eKE). An analogous high energy probe study has not yet been performed for  $I^- \cdot T$  clusters, but the laser photodissociation spectroscopy results confirm that  $I^-$  is produced from both sets of photoexcited clusters. We now consider the assignment of the origin of the iodide signal as well as the autodetachment signal from both  $I^- \cdot U$  and  $I^- \cdot T$  clusters.

For both  $I^- \cdot U$  and  $I^- \cdot T$  clusters, the VB anion appearance and fast decay dynamics in Fig. 7 match closely with the autodetachment depletion and recovery signal. It is also striking from the overlay of the one-color photoelectron spectra with the laser photodissociation results for  $I^-$  formation in Figs. 8c and 8d that the autodetachment signal tracks closely with the  $I^-$  photofragment production. Thus, it appears that  $I^-$  formation, autodetachment, and the VB anion share one common dynamical origin that is similar in nature between both sets of clusters.

Given that the excited state calculations for both  $I^- \cdot U$  and  $I^- \cdot T$  clusters find strong oscillator strength for a base-centered  $\pi-\pi^*$  excitation as a result of photoexcitation in this energy regime, we can begin by considering the possible ensuing relaxation and decay channels from an optical excitation of this nature. Specifically, two possibilities following  $\pi-\pi^*$  excitation that exist are IC to the  $I^- \cdot N$  ground state to yield cluster dissociation to produce  $I^-$ , as in Eq. 7a, and charge transfer from iodide to the base moiety to fill the hole in the  $\pi$  orbital, essentially creating a VB anion that may then undergo autodetachment (Eq. 7b).



We previously considered the possibility of formation of the VB anion in this excitation regime by charge transfer from iodide, but thought it unlikely given the  $<150$  fs appearance of the VB anion and the lack of orbital overlap between the  $I(5p)$  and  $\pi^*$  VB orbitals.<sup>26</sup> However, the calculated result that the  $\pi-\pi^*$  optical excitation is expected to dominate in this UV absorption region and the experimental result that the presence of autodetachment (and therefore the VB anion) tracks closely with the envelope of  $I^-$  formation are compelling evidence that  $\pi-\pi^*$  excitation is the origin of the observed dynamics. The calculated results described at the beginning of Section IIIB find some evidence that a  $I(5p) \rightarrow \sigma^*$  photoexcitation channel is active, and such a

$\sigma^*$  state may potentially couple more effectively with the VB state to facilitate its rapid formation. If the existence of a  $\sigma^*$  state is real and resembles that in Fig. 8g, photodetachment from this state would likely yield a narrow spectral profile given that this excited anion geometry is likely not significantly distorted from the neutral. However, the TRPES results find no evidence for the presence of another charged intermediate state. Moreover, it is clear from the time-resolved results for  $I^- \cdot T$  that the VB anion decays solely by autodetachment, and therefore does not produce the  $I^-$  signal measured by laser photodissociation spectroscopy. It thus seems unlikely that  $I(5p) \rightarrow \sigma^*$  photoexcitation is the source of the observed dynamics here.

It has also been previously suggested<sup>25</sup> that in the TRPES experiments, the pump pulse ejects the excess electron from the  $I^-$  moiety that is then captured by the nucleobase to form the VB anion in a two-step scattering type mechanism. This interpretation was offered before observation and characterization of the  $I^-$  channel. However, it now seems more likely that both autodetachment and  $I^-$  production originate from one common mechanism, rather than a combination of a scattering mechanism to create a VB anion that decays by autodetachment and a  $\pi-\pi^*$  excited state that relaxes by IC to produce  $I^-$ . Therefore, it appears that the strongest possibility for VB anion formation in this photoexcitation regime for both  $I^- \cdot U$  and  $I^- \cdot T$  is base-centered  $\pi-\pi^*$  excitation followed by prompt charge transfer from the iodide.

We can expect then that a mechanism as in Eq. 7a, or IC of the photoexcited state followed by cluster dissociation, is the origin of the  $I^-$  formation measured in this UV region. Thus, we conclude that in both  $I^- \cdot U$  and  $I^- \cdot T$ , photoexcitation from  $\sim 4.6$  eV – 4.8 eV creates a  $\pi-\pi^*$  excited state, some fraction of which may decay by IC to the  $I^- \cdot N$  ground state followed by dissociation to produce  $I^-$  (Eq. 7a), and another fraction of which may have charge transfer within the cross-correlation of the pump and probe laser pulses from the iodide moiety to produce a VB anion that then decays by autodetachment (Eq. 7b). Fig. 9 shows the approximate energies and ranges for the excited states of  $I^- \cdot U$  and summarizes these proposed pathways (blue arrows) resulting from higher energy photoexcitation of  $I^- \cdot U$ . Additionally, Fig. 9 shows the near-VDE photoexcitation pathways (black arrows) of  $I^- \cdot U$  as described in the earlier subsections of Section IIIB.

While this overall excitation and decay mechanism for the higher energy excitation regime is appealing, it is challenging to explain the rapid rate of charge transfer from iodide to the  $\pi$  orbital to form the VB anion in  $<150$  fs given the lack of orbital overlap. Additionally,  $I^- \cdot U$  exhibits long-lived dynamics that are not present in  $I^- \cdot T$ , and it is unclear why the  $I^- \cdot U$  VB anion exhibits both

fast and slow decay by autodetachment, although we have put forth such mechanistic explanations previously.<sup>23-25, 27</sup> A more extensive theoretical investigation into the nature and energetics of the photoexcited states accessible in this pump energy region may be needed to fully explain the mechanism of the VB anion formation as well as these differences exhibited here in the long-time dynamics of  $I^- \cdot U$  compared to  $I^- \cdot T$ .

### C. $I^- \cdot \text{Uracil} \cdot \text{H}_2\text{O}$

Microhydration of  $I^- \cdot U$  clusters, the step-wise addition of individual water molecules, provides insight into the role of water and solvation on the dynamics of electron attachment and photodissociation in these clusters. Anion photoelectron spectroscopy shows an increase in the electron affinity of pyrimidine nucleobases with the successive addition of water molecules,<sup>17</sup> and resonantly enhanced multiphoton ionization (REMPI) experiments find an increase in IC and photostability and decrease in excited state lifetimes with the addition of water to uracil and thymine.<sup>99, 100</sup> Previous  $U^- \cdot \text{H}_2\text{O}$  photoelectron spectra only show evidence for the VB anion,<sup>17, 41</sup> and suggest that the VB anion may be preferentially stabilized over the DB anion due to the interaction energy with water being higher with the increased density of the excess electron in the VB anion.<sup>20, 101</sup> We have recently investigated the dynamics of electron attachment and photodissociation in TRPES experiments on near-VDE photoexcited  $I^- \cdot U \cdot \text{H}_2\text{O}$  clusters.<sup>29</sup>

Single photon PES of  $I^- \cdot U \cdot \text{H}_2\text{O}$  finds the cluster VDE to be  $4.40 \text{ eV} \pm 0.05 \text{ eV}$  (Fig. 4d, peak A), in agreement with the calculated VDEs for a variety of  $I^- \cdot U \cdot \text{H}_2\text{O}$  conformers.<sup>29</sup> EOM-CCSD/aug-cc-pVDZ(-pp) excited state calculations carried out by our group on  $I^- \cdot U \cdot \text{H}_2\text{O}$  clusters, analogous to those results presented for  $I^- \cdot U$  above, also find three low-energy photoexcitation channels with considerable oscillator strength corresponding to excitation of the excess iodine ( $5p$ ) electron to a cluster DB orbital. No photodepletion experiments have been carried out for this cluster, but if the same energetic offset for  $I^- \cdot U$  is employed for  $I^- \cdot U \cdot \text{H}_2\text{O}$ , these three channels lie in the vicinity of the  $I^- \cdot U \cdot \text{H}_2\text{O}$  VDE. Thus, we may expect that in  $I^- \cdot U \cdot \text{H}_2\text{O}$ , pump excitation directly yields the DB anion as in  $I^- \cdot U$ .

TRPES of  $I^- \cdot U \cdot \text{H}_2\text{O}$  clusters photoexcited at  $4.38 \text{ eV}$ ,  $20 \text{ meV}$  below the VDE, show cross-correlation limited appearance of the DB anion, followed by appearance of the VB anion in  $400 \pm 140 \text{ fs}$  (Fig. 5d). The binding energy range for each of these features is notably  $\sim 0.2 \text{ eV}$  higher in

maximum eBE for each TNI than the corresponding TNIs of  $I^- \cdot U$  clusters, indicating that association of water with the  $I^- \cdot U$  cluster serves to energetically stabilize both the DB and VB anion.

The greatest accord in lifetimes between  $I^- \cdot U \cdot H_2O$  (-20 meV) and  $I^- \cdot U$  was found to be for  $I^- \cdot U$  (+30 meV).<sup>29</sup> The fast appearance of the DB anion is similar in both clusters, but the appearance of the VB anion in 400 fs is somewhat delayed compared to the approximately 220 fs VB anion rise in  $I^- \cdot U$ . This finite VB anion rise time may reflect partial DB to VB anion conversion, as has been suggested for  $I^- \cdot U$  clusters.<sup>25, 29</sup> The DB to VB anion conversion barrier for  $U^- \cdot H_2O$  has been calculated by Takayanagi and co-workers<sup>20</sup> to vary from approximately 18.6 – 130 meV depending on the specific binding site of  $H_2O$  around uracil. They have calculated the barrier to water-binding-site isomerization to be approximately 40-200 meV as well, and suggest that the water molecule may rearrange to a binding site that will lower the DB to VB conversion barrier. This water binding site rearrangement could delay the VB anion formation by approximately 100-200 fs, yielding the somewhat delayed VB formation in  $I^- \cdot U \cdot H_2O$  relative to  $I^- \cdot U$ , and therefore a more prominent DB to VB anion conversion, as seen in the  $I^- \cdot U \cdot H_2O$  DB anion decay and VB anion rise in Fig. 5d compared to the TNIs of  $I^- \cdot U$  in Fig. 5b.

Both TNIs of  $I^- \cdot U \cdot H_2O$  decay bi-exponentially in approximately 5 ps and 500 ps, and autodetachment is observed as a decay channel.<sup>29</sup> The  $I^- \cdot U \cdot H_2O$  DB anion fast and slow decay and the VB anion fast decay are quite similar to the  $I^- \cdot U$  (+30 meV) results, but the long-time decay component of the VB anion is considerably longer in  $I^- \cdot U \cdot H_2O$  (650 ps) than that of  $I^- \cdot U$  (80 ps). This may arise from the preferential stabilization of the VB anion over the DB anion upon the addition of water,<sup>20, 101</sup> effectively stabilizing the  $I^- \cdot U \cdot H_2O$  VB anion relative to autodetachment at longer times.

TRPES of  $I^- \cdot U \cdot H_2O$  with -20 meV pump excitation energy and a probe energy of 3.14 eV finds bi-exponential rise of  $I^-$  with time constants of  $6.7 \pm 3.8$  ps and  $320 \pm 30$  ps (Fig. 6d). Given the relatively similar bi-exponential DB and VB anion decay and similar  $I^-$  bi-exponential rise in near-VDE excited  $I^- \cdot U$  and  $I^- \cdot U \cdot H_2O$  clusters, these results indicate there is likely a congruent mechanism in both cluster systems for TNI decay to yield bi-exponential formation of the  $I^-$ . For both  $I^- \cdot U$  and  $I^- \cdot U \cdot H_2O$  clusters, we can thus expect that the  $I^-$  fast rise originates from IC of the DB anion to the anion ground state followed by evaporation of  $I^-$ , and the  $I^-$  slow rise from delayed ejection of  $I^-$  from VB anion IC and dissociation, as in Eq. 6. However, these 3.14 eV probe

experiments are not able to photodetach some possible photofragments such as  $I^- \cdot H_2O$  (VDE = 3.51 eV)<sup>102, 103</sup>, which could also act as an intermediate in the re-formation of  $I^-$ . TRPES experiments for  $I^- \cdot U \cdot H_2O$  with near-VDE pump and > 3.6 eV probe pulses to probe the possible appearance of  $I^- \cdot H_2O$  are currently underway in our laboratory, as well as  $\pi$ - $\pi^*$  pump excitation energy TRPES studies for  $I^- \cdot U \cdot H_2O$ .

#### D. $I^-$ -Adenine

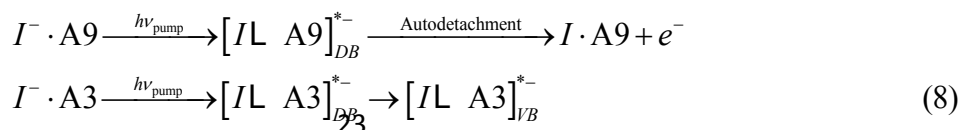
Adenine, a purine nucleobase, is also expected to be capable of supporting an excess electron in a DB state, although adenine anions have been less extensively studied than those of uracil or thymine. The biological adenine tautomer, A9, has a molecular dipole moment of 2.5-2.8 D,<sup>32, 33</sup> which is large enough to support a DB state.<sup>31, 104, 105</sup> The A9 VB anion, however, has been calculated to be adiabatically unbound<sup>106</sup> and only weakly vertically bound,<sup>28, 107</sup> if at all. However, some higher-lying non-canonical tautomers of adenine such as the A3 tautomer have been calculated to support a VB anion with a VDE of 0.686 eV.<sup>28</sup> Anion photoelectron spectroscopy studies by Bowen and co-workers have measured various gas phase anions of adenine,<sup>108, 109</sup> but neither DB nor VB anions of A9 were detected in these studies. Here, we present TRPES studies of the dynamics of TNI formation in near-VDE photoexcited  $I^- \cdot A$  complexes.<sup>28</sup>

The single photon photoelectron spectrum of  $I^- \cdot A$ , Fig. 4e, shows vertical detachment of the  $I^- \cdot A9$  complex at 3.96 eV, feature A, in agreement with CCSD/aug-cc-pVDZ(-pp) calculations for the cluster VDE.<sup>28</sup> A shoulder, feature A', is observed near 4.1 eV in the one color spectrum; we discuss possible origins for this shoulder below. TRPES studies for  $I^- \cdot A$  clusters were conducted with pump photon energies from -110 meV to +10 meV relative to the  $I^- \cdot A9$  VDE. At each of these excitation energies, both DB and VB anions were measured; the TRPES results for -60 meV photoexcitation are presented in Fig. 5e. At each pump excitation energy, a DB state is observed with a rise time of approximately 250 fs. At (and below) -60 meV photoexcitation, the DB anion decays mono-exponentially with a decay lifetime of approximately 11 ps, but at pump energies  $\geq$  -20 meV, the DB anion decays bi-exponentially in approximately 4 ps and 100-1000 ps. The VB anion, with a VDE of  $\sim$ 0.5 eV, appears in approximately 5-10 ps at each photoexcitation energy, with mono-exponential decay in approximately 60-100 ps. The close match-up of lifetimes of the DB anion fast decay and the VB anion rise time at all excitation energies is commensurate with the DB anion to VB anion conversion previously observed in

photoexcited  $I^- \cdot CH_3NO_2$  complexes. However, the observed VDE of  $\sim 0.5$  eV for the VB anion lies well above the calculated values for the A9 tautomer, which range from 0.03 eV-0.135 eV.<sup>28, 107</sup>

To assign these differing  $I^- \cdot A$  TNI dynamics at each pump excitation energy, it is important to consider the propensity of adenine to form low-lying non-canonical tautomers upon heating in the thermal desorption cluster source. CCSD/aug-cc-pVDZ(-pp) calculations have calculated the  $I^- \cdot A3$  VDE to be 4.15 eV,<sup>28</sup> which is in close agreement with the 4.11 eV A' shoulder feature observed in the one color photoelectron spectra in Fig. 4e. The low-lying A3 tautomer has a dipole moment of 4.7 D,<sup>33</sup> and thus it may contribute to the DB anion signal measured here. The A3 tautomer has also been calculated to have a VB anion with a positive adiabatic electron affinity,<sup>107</sup> for which the VDE has been calculated to be 0.686 eV.<sup>28</sup> Thus, it appears that both  $I^- \cdot A9$  and  $I^- \cdot A3$  tautomers contribute to the measured time-resolved signal, and it is necessary to distinguish the contributions of each to the observed dynamics.

The energetic landscape for the DB to VB anion interconversion has been calculated by Takayanagi and co-workers for the A9 and A3 tautomers, as well as interconversion from the A9 DB anion to form the A3 VB anion.<sup>28</sup> The calculated potential energy surfaces for these DB to VB anion transitions in and among A9 and A3 are presented in Fig. 10. It can be seen that the conversion in A9 has a high barrier and is nearly  $\sim 0.5$  eV endothermic, while the A3 tautomer DB to VB anion conversion is exothermic with a very modest barrier. Thus, the A3 tautomer is expected to have an energetic landscape similar to  $CH_3NO_2$ , for which the VB anion is the ground state and the conversion from the DB anion to the VB anion is exothermic and nearly barrierless. Based on the previously discussed calculated results that indicate an A9 VB anion is not expected to be bound and this calculated  $\sim 0.5$  eV barrier to A9 TNI partial conversion, the similar energetic landscape between  $CH_3NO_2$  and the A3 tautomer would suggest that the A3 tautomer is likely to be the species that undergoes the DB anion to VB anion conversion measured by TRPES. However, the bi-exponential DB anion decay dynamics measured here likely contain both tautomers, and it may be expected that the A9 tautomer, unable energetically to form the VB anion, will undergo autodetachment and give rise to the long-time decay component of the DB anion measured here. These dynamics are summarized in Eq. 8:





Given the similarities between the A3 tautomer and  $\text{CH}_3\text{NO}_2$ , it is interesting that the VB anion of near-VDE photoexcited  $\text{I}^- \cdot \text{CH}_3\text{NO}_2$  complexes exhibits bi-exponential decay in 2 ps (from internal conversion) and 1200 ps while that of  $\text{I}^- \cdot \text{A3}$  exhibits mono-exponential decay in  $\sim 60$ -100 ps. Although higher energy probe TRPES studies on  $\text{I}^- \cdot \text{A}$  have not been performed, this  $\sim 60$ -100 ps timescale may result from cluster internal conversion to dissociate to yield  $\text{I}^-$  rather than decay by autodetachment or H-atom loss as previously suggested,<sup>28</sup> although contributions from all of these channels are possible. We note that as a result of the presence of low-lying non-canonical tautomers upon heating, further TRPES studies for  $\text{I}^- \cdot \text{A}$ , iodide-cytosine ( $\text{I}^- \cdot \text{C}$ ) and iodide-guanine ( $\text{I}^- \cdot \text{G}$ ) have not been performed.

#### IV. SUMMARY AND OUTLOOK

TRPES of  $\text{I}^- \cdot \text{N}$  clusters has revealed the ultrafast formation and conversion of nucleobase TNIs thought to be important in reductive damage pathways in DNA. Following photoexcitation in the vicinity of the cluster VDE, the DB anion is found in some cases, as in  $\text{I}^- \cdot \text{A3}$ , to act as a doorway to the exothermic formation of the conventional VB anion. In other cases, as in  $\text{I}^- \cdot \text{U}$  and  $\text{I}^- \cdot \text{T}$ , the DB anion is the ground state and a greater energetic barrier to TNI interconversion appears to yield only partial conversion. These TNIs are both susceptible to autodetachment, but also appear to participate in cluster photodissociation in 10s of ps by internal conversion to the ground state to eventually re-form  $\text{I}^-$ . Base-centered  $\pi$ - $\pi^*$  photoexcitation also appears to lead to cluster decay by internal conversion followed by dissociation to form  $\text{I}^-$ , and may also coincide with VB anion formation by intracuster charge transfer following  $\pi$ - $\pi^*$  excitation with subsequent decay by autodetachment. However, more theoretical work is needed to fully understand the dynamics resulting from  $\pi$ - $\pi^*$  photoexcitation in these anionic clusters.

Ongoing work in our laboratory is aimed at the continued microhydration of  $\text{I}^- \cdot \text{N}$  clusters. Microsolvation is expected to eventually stabilize the VB anion and fully suppress the DB anion, and it remains to be seen how many water molecules must be added before this transition occurs. The stepwise addition of individual water molecules building up to a solvation shell will also allow for comparison between gas-phase dynamics of nucleobases and those recorded in bulk solution. In this regard, TRPES experiments in our group<sup>110</sup> and elsewhere<sup>111, 112</sup> on the dynamics of nucleic acid constituents in liquid water microjets are of particular interest.

The future implementation of a new cluster source, such as one based on electrospray ionization,<sup>62</sup> will enable TRPES of nucleobases commonly prone to tautomerization upon heating, such as cytosine and guanine, in addition to the study of larger biomolecules such as nucleosides and nucleotides. Dessent et al.<sup>42</sup> have recently measured distinct photoabsorption and photofragmentation profiles in  $I^- \cdot C$  clusters in which there is relatively flat and intense  $I^-$  production across the entire region above the VDE. Electrospray ionization could thus similarly be used to generate clusters of iodide-uridine or iodide-uridine-monophosphate, among others, with the ultimate goal of inducing electron attachment and monitoring not only the initial site of electron attachment and the TNI dynamics, but also probing photofragment formation to measure the identities and timescales for formation of photodissociation products in these larger nucleic acid constituents.

## CONFLICTS OF INTEREST

There are no conflicts of interest to declare.

## ACKNOWLEDGEMENTS

This research was funded by the National Science Foundation under Grant No. CHE-1663832. A.K. acknowledges Government support awarded by DoD, Air Force Office of Scientific Research, National Defense Science and Engineering Graduate (NDSEG) Fellowship, 32 CFR 168a. D.M.N. thanks the many graduate students and postdoctoral fellows who carried out the work in his laboratory that is reported here.

## References

1. B. Boudaiffa, P. Cloutier, D. Hunting, M. A. Huels and L. Sanche, *Science*, 2000, 287, 1658-1660.
2. R. Barrios, P. Skurski and J. Simons, *J. Phys. Chem. B*, 2002, 106, 7991-7994.
3. J. Simons, *Accounts Chem. Res.*, 2006, 39, 772-779.
4. H.-Y. Chen, P.-Y. Yang, H.-F. Chen, C.-L. Kao and L.-W. Liao, *J. Phys. Chem. B*, 2014, 118, 11137-11144.
5. J. Berdys, I. Anusiewicz, P. Skurski and J. Simons, *J. Am. Chem. Soc.*, 2004, 126, 6441-6447.
6. J. Berdys, P. Skurski and J. Simons, *J. Phys. Chem. B*, 2004, 108, 5800-5805.
7. E. Alizadeh and L. Sanche, *Chem. Rev.*, 2012, 112, 5578-5602.
8. C. Desfrancois, H. Abdoul-Carime and J.-P. Schermann, *Int. J. Mod. Phys. B*, 1996, 10, 1339-1395.
9. R. A. Bachorz, W. Klopper, M. Gutowski, X. Li and K. H. Bowen, *J. Chem. Phys.*, 2008, 129, 054309.
10. P. D. Burrow, G. A. Gallup, A. M. Scheer, S. Denifl, S. Ptasinska, T. D. Märk and P. Scheier, *J. Chem. Phys.*, 2006, 124, 124310.
11. G. Hanel, B. Gstir, S. Denifl, P. Scheier, M. Probst, B. Farizon, M. Farizon, E. Illenberger and T. D. Märk, *Phys. Rev. Lett.*, 2003, 90.
12. S. Ptasinska, S. Denifl, S. Gohlke, P. Scheier, E. Illenberger and T. D. Märk, *Angew. Chem. Int. Ed.*, 2006, 45, 1893-1896.
13. S. Denifl, S. Ptasinska, G. Hanel, B. Gstir, M. Probst, P. Scheier and T. D. Märk, *J. Chem. Phys.*, 2004, 120, 6557-6565.
14. G. A. Gallup and I. I. Fabrikant, *Phys. Rev. A*, 2011, 83.
15. S. Denifl, P. Sulzer, F. Zappa, S. Moser, B. Kraeutler, O. Echt, D. K. Bohme, T. D. Märk and P. Scheier, *Int. J. Mass. Spectrom.*, 2008, 277, 296-299.
16. J. H. Hendricks, S. A. Lyapustina, H. L. de Clercq, J. T. Snodgrass and K. H. Bowen, *J. Chem. Phys.*, 1996, 104, 7788-7791.
17. J. Schiedt, R. Weinkauff, D. M. Neumark and E. W. Schlag, *Chem. Phys.*, 1998, 239, 511-524.
18. T. Sommerfeld, *J. Phys. Chem. A*, 2004, 108, 9150-9154.
19. T. Takayanagi, T. Asakura and H. Motegi, *J. Phys. Chem. A*, 2009, 113, 4795-4801.
20. H. Motegi and T. Takayanagi, *J. Mol. Struct.*, 2009, 907, 85-92.
21. Y. Yokoi, K. Kano, Y. Minoshima and T. Takayanagi, *Comput. Theor. Chem.*, 2014, 1046, 99-106.
22. J. Gu, J. Leszczynski and H. F. Schaefer, *Chem. Rev.*, 2012, 112, 5603-5640.
23. M. A. Yandell, S. B. King and D. M. Neumark, *J. Am. Chem. Soc.*, 2013, 135, 2128-2131.
24. S. B. King, M. A. Yandell and D. M. Neumark, *Faraday Discuss.*, 2013, 163, 59-72.
25. S. B. King, M. A. Yandell, A. B. Stephansen and D. M. Neumark, *J. Chem. Phys.*, 2014, 141, 224310.
26. W.-L. Li, A. Kunin, E. Matthews, N. Yoshikawa, C. E. H. Dessent and D. M. Neumark, *J. Chem. Phys.*, 2016, 145, 044319.
27. S. B. King, A. B. Stephansen, Y. Yokoi, M. A. Yandell, A. Kunin, T. Takayanagi and D. M. Neumark, *J. Chem. Phys.*, 2015, 143.

28. A. B. Stephansen, S. B. King, Y. Yokoi, Y. Minoshima, W.-L. Li, A. Kunin, T. Takayanagi and D. M. Neumark, *J. Chem. Phys.*, 2015, 143, 104308.
29. A. Kunin, W.-L. Li and D. M. Neumark, *J. Chem. Phys.*, 2018, 149, 084301.
30. R. N. Compton, H. S. Carman, C. Desfrancois, H. Abdoulcarimine, J. P. Schermann, J. H. Hendricks, S. A. Lyapustina and K. H. Bowen, *J. Chem. Phys.*, 1996, 105, 3472-3478.
31. O. H. Crawford, *Mol. Phys.*, 1971, 20, 585-591.
32. S. Carles, F. Lecomte, J. P. Schermann and C. Desfrancois, *J. Phys. Chem. A*, 2000, 104, 10662-10668.
33. M. Hanus, M. Kabelac, J. Rejnek, F. Ryjacek and P. Hobza, *J. Phys. Chem. B*, 2004, 108, 2087-2097.
34. I. Kulakowska, M. Geller, B. Lesyng and K. L. Wierzchowski, *Biochim. Biophys. Acta, Nucleic Acids Protein Synth.*, 1974, 361, 119-130.
35. J. Simons, *J. Phys. Chem. A*, 2008, 112, 6401-6511.
36. R. A. Bachorz, W. Klopper and M. Gutowski, *J. Chem. Phys.*, 2007, 126, 085101.
37. C. Desfrancois, H. AbdoulCarime and J. P. Schermann, *J. Chem. Phys.*, 1996, 104, 7792-7794.
38. O. Dolgounitcheva, V. G. Zakrzewski and J. V. Ortiz, *Chem. Phys. Lett.*, 1999, 307, 220-226.
39. O. Dolgounitcheva, V. G. Zakrzewski and J. V. Ortiz, *J. Phys. Chem. A*, 2001, 105, 8782-8786.
40. D. Svozil, T. Frigato, Z. Havlas and P. Jungwirth, *Phys. Chem. Chem. Phys.*, 2005, 7, 840-845.
41. J. H. Hendricks, S. A. Lyapustina, H. L. de Clercq and K. H. Bowen, *J. Chem. Phys.*, 1998, 108, 8-11.
42. E. Matthews, R. Cercola, G. Mensa-Bonsu, D. M. Neumark and C. E. H. Dessent, *J. Chem. Phys.*, 2018, 148, 084304.
43. R. Improta, F. Santoro and L. Blancafort, *Chem. Rev.*, 2016, 116, 3540-3593.
44. K. Kleiner, D. Nachtigallová and M. S. de Vries, *Int. Rev. Phys. Chem.*, 2013, 32, 308-342.
45. C. T. Middleton, K. de La Harpe, C. Su, Y. K. Law, C. E. Crespo-Hernández and B. Kohler, *Annu. Rev. Phys. Chem.*, 2009, 60, 217-239.
46. R. J. Peláez, C. Blondel, C. Delsart and C. Drag, *J. Phys. B-At. Mol. Opt.*, 2009, 42, 125001.
47. H.-T. Liu, C.-G. Ning, D.-L. Huang and L.-S. Wang, *Angew. Chem. Int. Edit.*, 2014, 53, 2464-2468.
48. B. F. Parsons, S. M. Sheehan, T. A. Yen, D. M. Neumark, N. Wehres and R. Weinkauff, *Phys. Chem. Chem. Phys.*, 2007, 9, 3291-3297.
49. H. Xie and Z. Cao, *Int. J. Quantum Chem.*, 2006, 107, 1261-1269.
50. C. C. Hayden and A. Stolow, in *Photoionization and Photodetachment*, WORLD SCIENTIFIC, 2000, vol. Volume 10, pp. 91-126.
51. D. M. Neumark, *Annu. Rev. Phys. Chem.*, 2001, 52, 255-277.
52. T. Suzuki and B. J. Whitaker, *Int. Rev. Phys. Chem.*, 2001, 20, 313-356.
53. A. Stolow, *Annu. Rev. Phys. Chem.*, 2003, 54, 89-119.
54. A. Stolow, *Int. Rev. Phys. Chem.*, 2003, 22, 377-405.
55. A. Stolow, A. E. Bragg and D. M. Neumark, *Chem. Rev.*, 2004, 104, 1719-1758.
56. T. Suzuki, in *Modern Trends in Chemical Reaction Dynamics*, WORLD SCIENTIFIC, 2004, vol. Volume 14, pp. 529-578.

57. M. Wollenhaupt, V. Engel and T. Baumert, *Annu. Rev. Phys. Chem.*, 2004, 56, 25-56.
58. T. Suzuki, *Annu. Rev. Phys. Chem.*, 2006, 57, 555-592.
59. J. R. R. Verlet, *Chem. Soc. Rev.*, 2008, 37, 505-517.
60. A. Stolow and J. G. Underwood, *Adv. Chem. Phys.*, 2008, DOI: doi:10.1002/9780470259498.ch6.
61. V. G. Stavros and J. R. R. Verlet, *Annu. Rev. Phys. Chem.*, 2016, 67, 211-232.
62. C. S. Anstöter, J. N. Bull and J. R. R. Verlet, *Int. Rev. Phys. Chem.*, 2016, 35, 509-538.
63. A. V. Davis, R. Wester, A. E. Bragg and D. M. Neumark, *J. Chem. Phys.*, 2003, 118, 999-1002.
64. A. E. Bragg, J. R. R. Verlet, A. Kammrath, O. Cheshnovsky and D. M. Neumark, *J. Am. Chem. Soc.*, 2005, 127, 15283-15295.
65. W. C. Wiley and I. H. McLaren, *Rev. Sci. Instrum.*, 1955, 26, 1150-1157.
66. A. Eppink and D. H. Parker, *Rev. Sci. Instrum.*, 1997, 68, 3477-3484.
67. V. Dribinski, A. Ossadtchi, V. Mandelshtam and H. Reisler, *Rev. Sci. Instrum.*, 2002, 73, 2634-2642.
68. M. J. Frisch, G. W. Trucks, H. B. Schlegel, G. E. Scuseria, M. A. Robb, J. R. Cheeseman, J. Montgomery, J. A., T. Vreven, K. N. Kudin, J. C. Burant, J. M. Millam, S. S. Iyengar, J. Tomasi, V. Barone, B. Mennucci, M. Cossi, G. Scalmani, N. Rega, G. A. Petersson, H. Nakatsuji, M. Hada, M. Ehara, K. Toyota, R. Fukuda, J. Hasegawa, M. Ishida, T. Nakajima, Y. Honda, O. Kitao, H. Nakai, M. Klene, X. Li, J. E. Knox, H. P. Hratchian, J. B. Cross, V. Bakken, C. Adamo, J. Jaramillo, R. Gomperts, R. E. Stratmann, O. Yazyev, A. J. Austin, R. Cammi, C. Pomelli, J. W. Ochterski, P. Y. Ayala, K. Morokuma, G. A. Voth, P. Salvador, J. J. Dannenberg, V. G. Zakrzewski, S. Dapprich, A. D. Daniels, M. C. Strain, O. Farkas, D. K. Malick, A. D. Rabuck, K. Raghavachari, J. B. Foresman, J. V. Ortiz, Q. Cui, A. G. Baboul, S. Clifford, J. Cioslowski, B. B. Stefanov, G. Liu, A. Liashenko, P. Piskorz, I. Komaromi, R. L. Martin, D. J. Fox, T. Keith, M. A. Al-Laham, C. Y. Peng, A. Nanayakkara, M. Challacombe, P. M. W. Gill, B. Johnson, W. Chen, M. W. Wong, C. Gonzalez and J. A. Pople, Gaussian, Inc., Wallingford, CT, USA, Revision D.02 edn., 2004.
69. M. J. Frisch, G. W. Trucks, H. B. Schlegel, G. E. Scuseria, M. A. Robb, J. R. Cheeseman, G. Scalmani, V. Barone, B. Mennucci, G. A. Petersson, H. Nakatsuji, M. Caricato, X. Li, H. P. Hratchian, A. F. Izmaylov, J. Bloino, G. Zheng, J. L. Sonnenberg, M. Hada, M. Ehara, K. Toyota, R. Fukuda, J. Hasegawa, M. Ishida, T. Nakajima, Y. Honda, O. Kitao, H. Nakai, T. Vreven, J. A. Montgomery Jr., J. E. Peralta, F. Ogliaro, M. J. Bearpark, J. Heyd, E. N. Brothers, K. N. Kudin, V. N. Staroverov, R. Kobayashi, J. Normand, K. Raghavachari, A. P. Rendell, J. C. Burant, S. S. Iyengar, J. Tomasi, M. Cossi, N. Rega, N. J. Millam, M. Klene, J. E. Knox, J. B. Cross, V. Bakken, C. Adamo, J. Jaramillo, R. Gomperts, R. E. Stratmann, O. Yazyev, A. J. Austin, R. Cammi, C. Pomelli, J. W. Ochterski, R. L. Martin, K. Morokuma, V. G. Zakrzewski, G. A. Voth, P. Salvador, J. J. Dannenberg, S. Dapprich, A. D. Daniels, Ö. Farkas, J. B. Foresman, J. V. Ortiz, J. Cioslowski and D. J. Fox, Gaussian, Inc., Wallingford, CT, USA, 2009.
70. A. Martinez, O. Dolgounitcheva, V. G. Zakrzewski and J. V. Ortiz, *J. Phys. Chem. A*, 2008, 112, 10399-10404.
71. T. H. Dunning, *J. Chem. Phys.*, 1989, 90, 1007-1023.
72. K. A. Peterson, B. C. Shepler, D. Figgen and H. Stoll, *J. Phys. Chem. A*, 2006, 110, 13887.
73. M. A. Yandell, S. B. King and D. M. Neumark, *J. Chem. Phys.*, 2014, 140, 184317.

74. A. D. McLean and G. S. Chandler, *J. Chem. Phys.*, 1980, 72, 5639-5648.
75. A. Bergner, M. Dolg, W. Küchle, H. Stoll and H. Preuß, *Mol. Phys.*, 1993, 80, 1431-1441.
76. R. Krishnan, J. S. Binkley, R. Seeger and J. A. Pople, *J. Chem. Phys.*, 1980, 72, 650-654.
77. A. D. Becke, *J. Chem. Phys.*, 1993, 98, 5648-5652.
78. T. Clark, J. Chandrasekhar, G. W. Spitznagel and P. V. R. Schleyer, *J. Comput. Chem.*, 1983, 4, 294-301.
79. M. J. Frisch, J. A. Pople and J. S. Binkley, *J. Chem. Phys.*, 1984, 80, 3265-3269.
80. A. Kunin, W.-L. Li and D. M. Neumark, *Phys. Chem. Chem. Phys.*, 2016, 18, 33226-33232.
81. T. Beyer and D. F. Swinehart, *Commun. Acm*, 1973, 16, 379-379.
82. S. E. Stein and B. S. Rabinovitch, *J. Chem. Phys.*, 1973, 58, 2438-2445.
83. C. E. H. Dessent, J. Kim and M. A. Johnson, *Faraday Discuss.*, 2000, 115, 395-406.
84. F. Lecomte, S. Carles, C. Desfrancois and M. A. Johnson, *J. Chem. Phys.*, 2000, 113, 10973-10977.
85. C. L. Adams, H. Schneider, K. M. Ervin and J. M. Weber, *J. Chem. Phys.*, 2009, 130.
86. J. E. Sansonetti and W. C. Martin, *J. Phys. Chem. Ref. Data*, 2005, 34, 1559-2259.
87. J. Simons, *J. Am. Chem. Soc.*, 1981, 103, 3971-3976.
88. P. K. Acharya, R. A. Kendall and J. Simons, *J. Am. Chem. Soc.*, 1984, 106, 3402-3407.
89. E. E. B. Campbell and R. D. Levine, *Annu. Rev. Phys. Chem.*, 2000, 51, 65-98.
90. J. U. Andersen, E. Bonderup and K. Hansen, *J. Phys. B*, 2002, 35, R1.
91. R. B. Metz, D. R. Cyr and D. M. Neumark, *J. Phys. Chem.*, 1991, 95, 2900-2907.
92. W. L. Hase, *Science*, 1994, 266, 998-1002.
93. J. Xie, R. Otto, J. Mikosch, J. Zhang, R. Wester and W. L. Hase, *Accts. Chem. Res.*, 2014, 47, 2960-2969.
94. M. L. Chabiny, S. L. Craig, C. K. Regan and J. I. Brauman, *Science*, 1998, 279, 1882.
95. H. Wang, G. H. Peslherbe and W. L. Hase, *J. Am. Chem. Soc.*, 1994, 116, 9644-9651.
96. G. H. Peslherbe, H. Wang and W. L. Hase, *J. Chem. Phys.*, 1995, 102, 5626-5635.
97. K. Mazurkiewicz, R. A. Bachorz, M. Gutowski and J. Rak, *J. Phys. Chem. B*, 2006, 110, 24696-24707.
98. N. A. Oyler and L. Adamowicz, *J. Phys. Chem.*, 1993, 97, 11122-11123.
99. Y. He, C. Wu and W. Kong, *J. Phys. Chem. A*, 2003, 107, 5145-5148.
100. Y. He, C. Wu and W. Kong, *J. Phys. Chem. A*, 2004, 108, 943-949.
101. C. A. Morgado, K. Y. Pichugin and L. Adamowicz, *Phys. Chem. Chem. Phys.*, 2004, 6, 2758-2762.
102. G. Markovich, R. Giniger, M. Levin and O. Cheshnovsky, *J. Chem. Phys.*, 1991, 95, 9416-9419.
103. G. Markovich, S. Pollack, R. Giniger and O. Cheshnovsky, *J. Chem. Phys.*, 1994, 101, 9344-9353.
104. G. L. Gutsev and L. Adamowicz, *Chem. Phys. Lett.*, 1995, 235, 377-381.
105. G. L. Gutsev and L. Adamowicz, *J. Phys. Chem.*, 1995, 99, 13412-13421.
106. D. Roca-Sanjuán, M. Merchan, L. Serrano-Andres and M. Rubio, *J. Chem. Phys.*, 2008, 129, 095104.
107. E. D. Raczyńska, M. Makowski, K. Zientara-Rytter, K. Kolczyńska, T. M. Stepniowski and M. Hallmann, *J. Phys. Chem. A*, 2013, 117, 1548-1559.
108. M. Haranczyk, M. Gutowski, X. Li and K. H. Bowen, *Proc. Natl. Acad. Sci. U.S.A.*, 2007, 104, 4804-4807.

109. X. Li, K. H. Bowen, M. Haranczyk, R. A. Bachorz, K. Mazurkiewicz, J. Rak and M. Gutowski, *J. Chem. Phys.*, 2007, 127, -.
110. H. L. Williams, B. A. Erickson and D. M. Neumark, *J. Chem. Phys.*, 2018, 148.
111. F. Buchner, H. H. Ritze, J. Lahl and A. Lubcke, *Phys. Chem. Chem. Phys.*, 2013, 15, 11402-11408.
112. F. Buchner, A. Nakayama, S. Yamazaki, H. H. Ritze and A. Lubcke, *J. Am. Chem. Soc.*, 2015, 137, 2931-2938.

Table I. A summary of calculated anion ground state structures and neutral dipole moments for the  $\Gamma^- \cdot \text{N}$  cluster systems examined in this work. The neutral dipole moment ( $\mu$ ) is reported at the geometry of the ground state anion. Reported VDEs are experimentally measured by anion PES, all  $\pm 0.05$  eV error. See cited references for specific computational details.

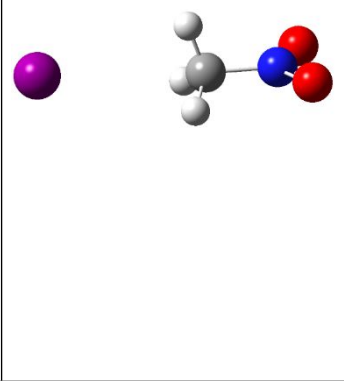
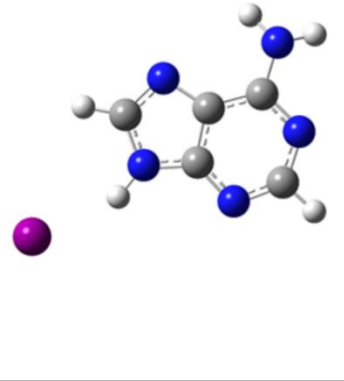
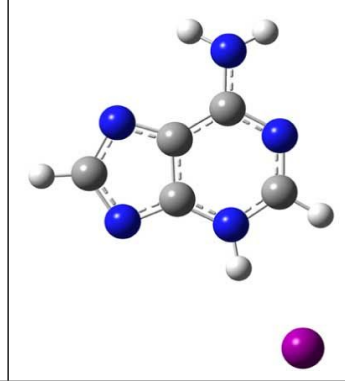
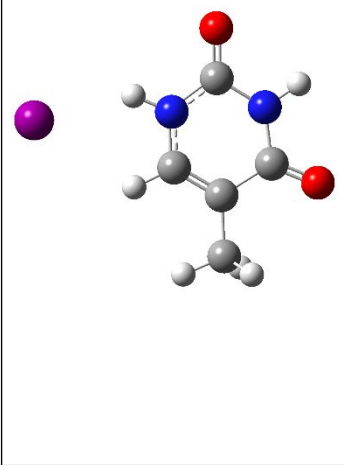
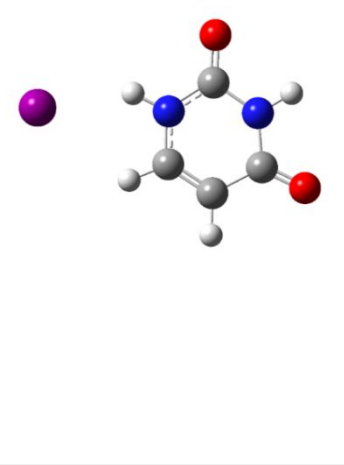
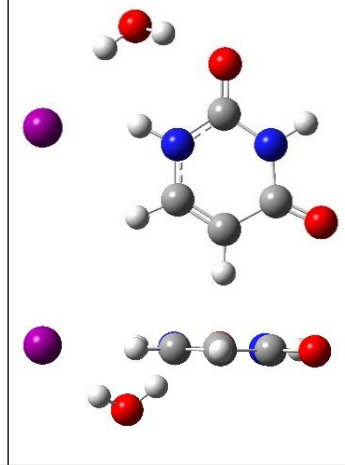
			
Cluster	$\Gamma^- \cdot \text{CH}_3\text{NO}_2$	$\Gamma^- \cdot \text{A9}$	$\Gamma^- \cdot \text{A3}$
VDE (eV)	3.60 eV	3.96 eV	4.11 eV
Neutral $\mu$ (D)	4.62 D	4.0 D <sup>28</sup>	5.6 D <sup>28</sup>
			
Cluster	$\Gamma^- \cdot \text{T}$	$\Gamma^- \cdot \text{U}$	$\Gamma^- \cdot \text{U} \cdot \text{H}_2\text{O}$
VDE (eV)	4.05 eV	4.11 eV	4.40 eV
Neutral $\mu$ (D)	6.23 D <sup>27</sup>	6.48 D <sup>27</sup>	6.93 D <sup>29</sup>



Figure 1. Photoelectron spectra of a) the uracil DB anion and b) the  $U^- \cdot H_2O$  VB anion. The  $U^-$  DB anion exhibits a spectrum with a very narrow peak at very low binding energy, characteristic of DB anions, while the  $U^- \cdot H_2O$  VB anion exhibits a broad feature covering higher eBEs. Adapted from Hendricks *et al.*, J. Chem. Phys. **108**, 1 (1998), with the permission of AIP Publishing.

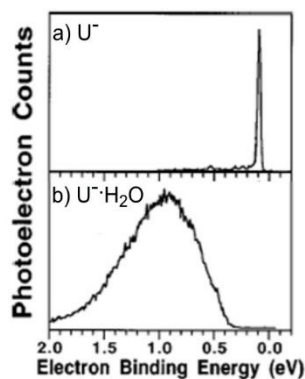


Figure 2. Example scheme for a) anion photoelectron spectroscopy and b) time-resolved photoelectron spectroscopy. Anion\* is used to indicate the photoexcited state. The blue lines indicate the resultant kinetic energies of the photodetached electrons.

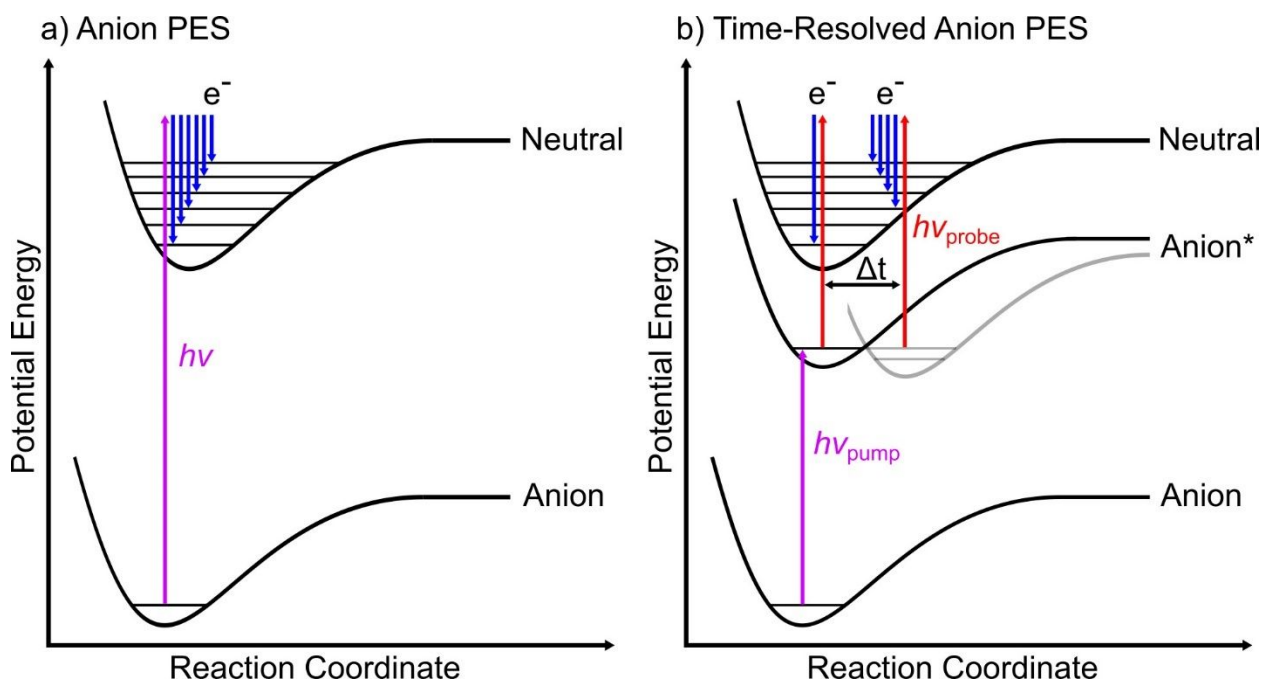


Figure 3. Diagram of the TRPES apparatus employed in this work.

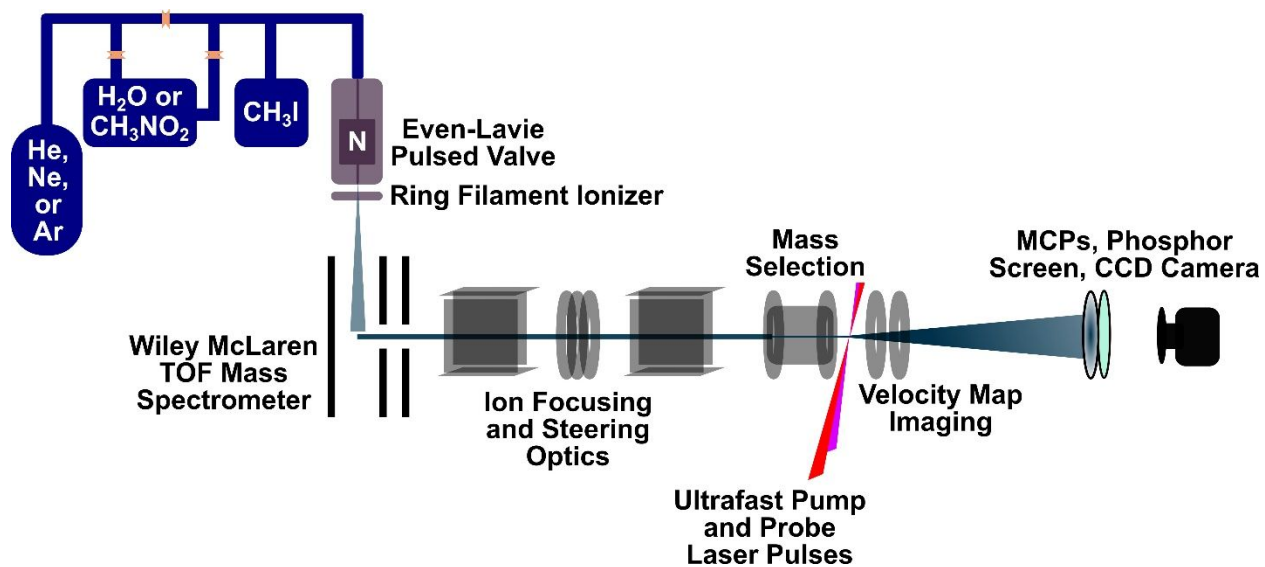


Figure 4. Single photon photoelectron spectra for a)  $\text{I}^- \cdot \text{CH}_3\text{NO}_2$  with 4.68 eV; b)  $\text{I}^- \cdot \text{U}$  with 5.30 eV in blue, 4.92 eV in red, 4.68 eV in purple, and 4.51 eV in orange; c)  $\text{I}^- \cdot \text{T}$  with 5.30 eV in blue, 4.87 eV in red, 4.78 eV in purple, 4.68 eV in orange, 4.59 eV in green, and 4.51 eV in black; d)  $\text{I}^- \cdot \text{U} \cdot \text{H}_2\text{O}$  with 4.74 eV; and e)  $\text{I}^- \cdot \text{A}$  with 4.52 eV. “A” denotes vertical detachment to the lower spin orbit state of the iodine-containing complex ( $\text{I}(^2\text{P}_{3/2}) \cdot \text{N}$ ) (with A’ shoulder for the detachment of two tautomers of adenine), “B” denotes detachment to the upper spin orbit state ( $\text{I}(^2\text{P}_{1/2}) \cdot \text{N}$ ), and “C” denotes autodetachment. (b) and (c) are adapted from Ref. 24 with permission from the Royal Society of Chemistry. (d) is reproduced from Kunin *et al.*, *J. Chem. Phys.* **149**, 084301 (2018), with the permission of AIP Publishing. (e) is adapted from Stephansen *et al.*, *J. Chem. Phys.* **143**, 104308 (2015), with the permission of AIP Publishing.

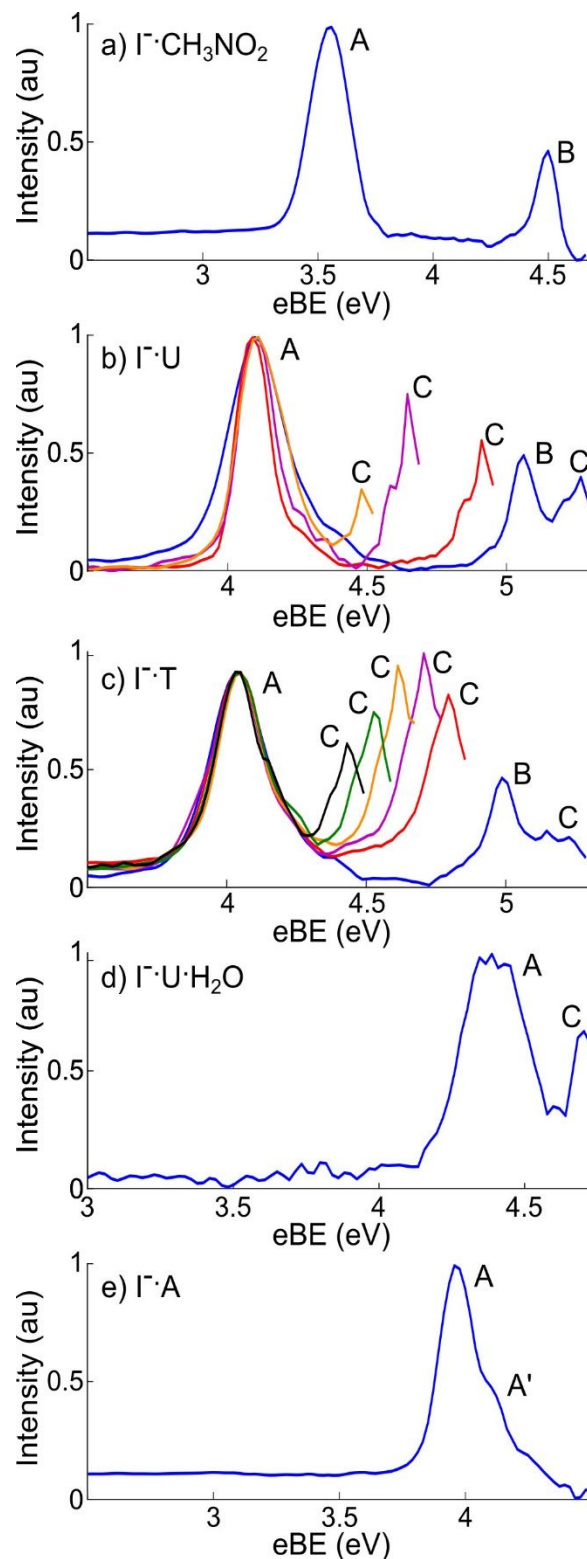


Figure 5. TRPE spectra and DB anion (feature A, blue) and VB anion (feature B, red) integrated intensities at both early times and long delay times for a)  $\text{I}^- \cdot \text{CH}_3\text{NO}_2$  photoexcited at +0 meV; b)  $\text{I}^- \cdot \text{U}$  photoexcited at +30 meV; c)  $\text{I}^- \cdot \text{T}$  photoexcited at +20 meV; d)  $\text{I}^- \cdot \text{U} \cdot \text{H}_2\text{O}$  photoexcited at -20 meV; and e)  $\text{I}^- \cdot \text{A}$  photoexcited at -60 meV. (a) is adapted from Yandell *et al.*, *J. Chem. Phys.* **140**, 184317 (2014), with the permission of AIP Publishing. (b) is adapted from King *et al.*, *J. Chem. Phys.* **141**, 224310 (2014), with the permission of AIP Publishing. (c) is adapted from King *et al.*, *J. Chem. Phys.* **143**, 024312 (2015), with the permission of AIP Publishing. (d) is reproduced from Kunin *et al.*, *J. Chem. Phys.* **149**, 084301 (2018), with the permission of AIP Publishing. (e) is adapted from Stephansen *et al.*, *J. Chem. Phys.* **143**, 104308 (2015), with the permission of AIP Publishing.

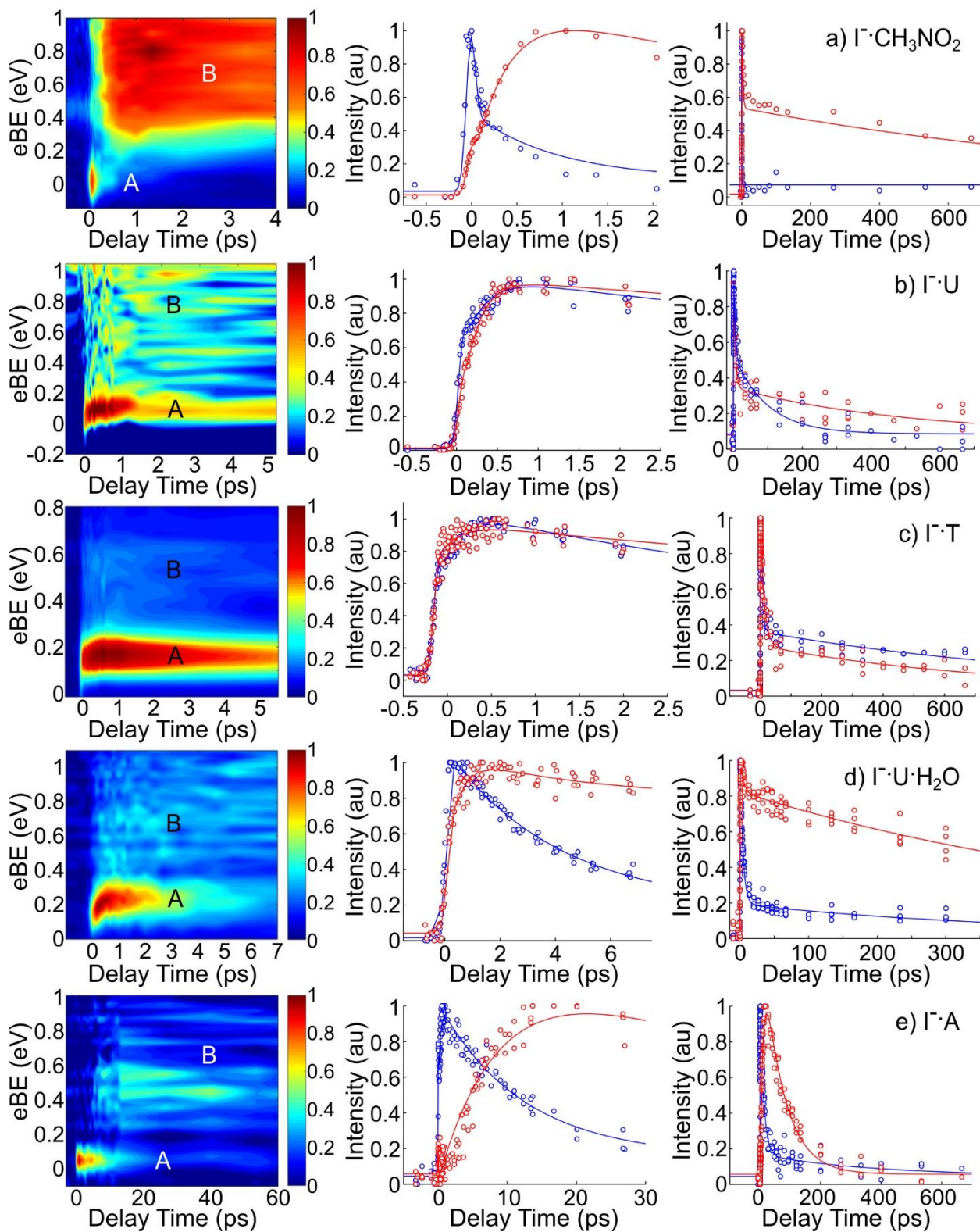


Figure 6. Iodide rise times for a)  $\text{I}^- \cdot \text{CH}_3\text{NO}_2$ , b)  $\text{I}^- \cdot \text{U}$  photoexcited -80 meV below the VDE, c)  $\text{I}^- \cdot \text{U}$  photoexcited at +610 meV (4.72 eV), and d)  $\text{I}^- \cdot \text{U} \cdot \text{H}_2\text{O}$  near-VDE pump. (a) is adapted from Ref. 80 with permission from the PCCP Owner Societies. (b) and (c) are adapted from Li *et al.*, J. Chem. Phys. **145**, 044319 (2016), with the permission of AIP Publishing. (d) is reproduced from Kunin *et al.*, J. Chem. Phys. **149**, 084301 (2018), with the permission of AIP Publishing.

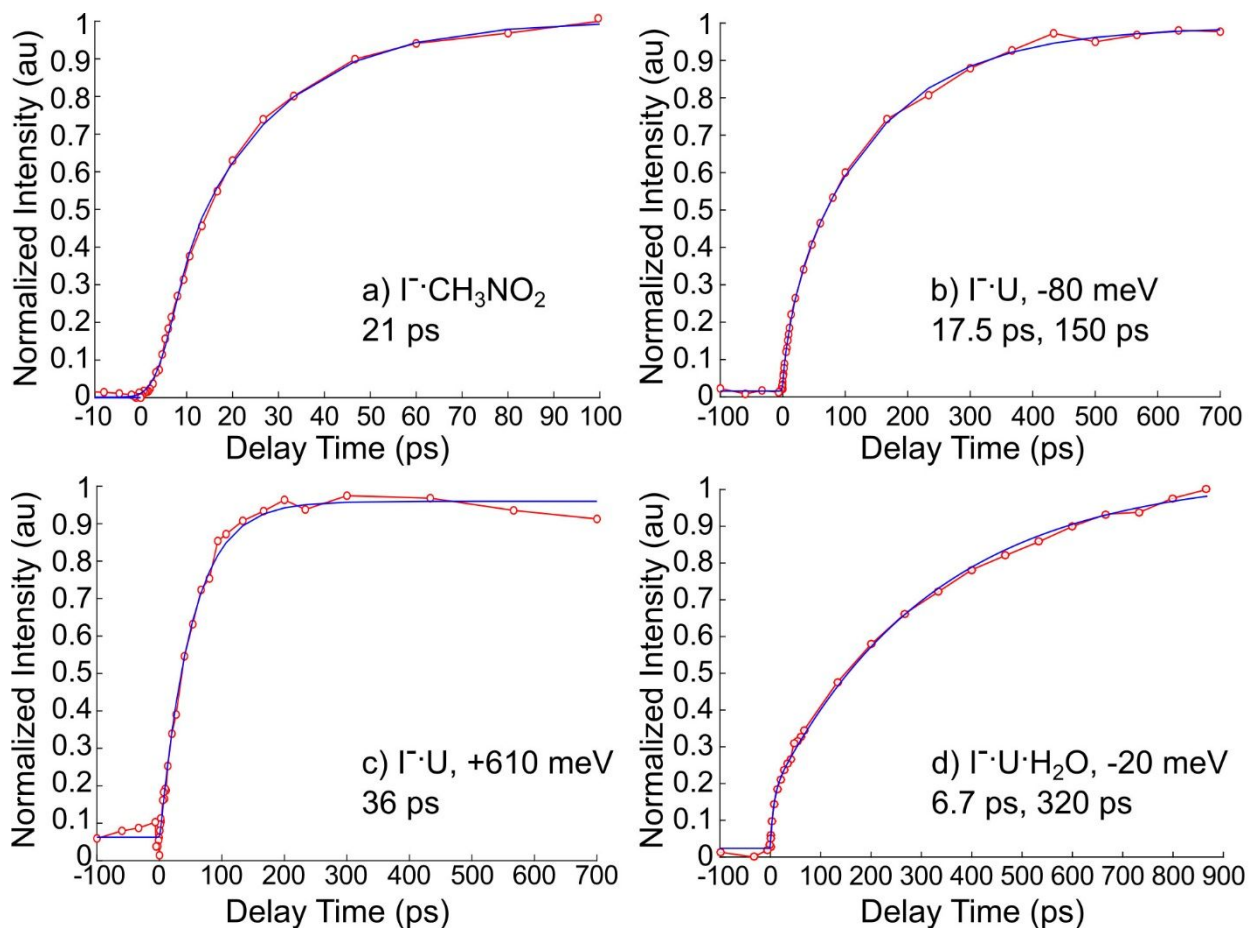


Figure 7. TRPE spectra and VB anion (red) and autodetachment (black) integrated intensities at both early times and long delay times for a)  $\Gamma^- \cdot \text{U}$  photoexcited at 4.69 eV; b)  $\Gamma^- \cdot \text{T}$  photoexcited at 4.69 eV. (a) is reprinted with permission from Yandell *et al.*, J. Am. Chem. Soc. **135**, 2128 (2013). Copyright 2013 American Chemical Society. (b) is adapted from Ref. 24 with permission from the Royal Society of Chemistry.

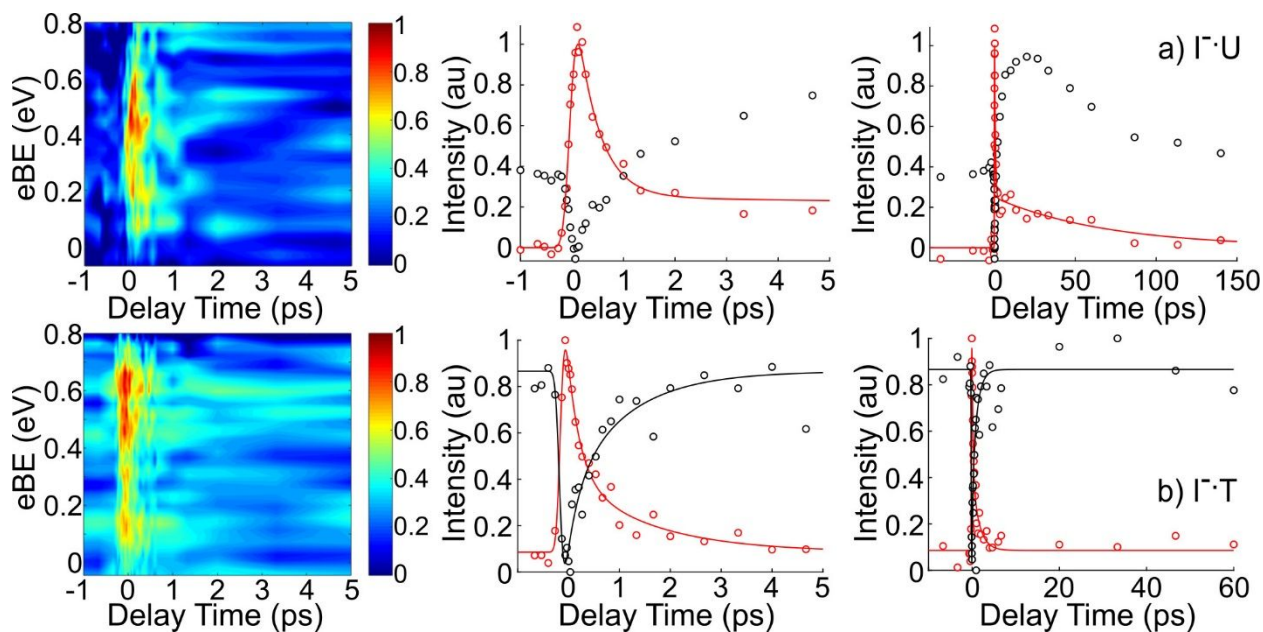


Figure 8. An overlay of the one color photoelectron spectra from Fig. 4b) for  $I^- \cdot U$  and Fig. 4c) for  $I^- \cdot T$  with the laser photodissociation spectroscopy results from Ref. 42. a) Photodepletion (absorption) for  $I^- \cdot U$  clusters photoexcited between 3.6 and 5.3 eV and b) for  $I^- \cdot T$  clusters. c) Formation of  $I^-$  from photoexcited  $I^- \cdot U$  clusters and d) formation of  $I^-$  from photoexcited  $I^- \cdot T$  clusters. Photoelectron spectra are normalized to match the photodissociation data (black dots). e) EOM-CCSD/aug-cc-pVDZ(-pp) calculated image of the  $I^- \cdot U$  DB orbital and f) for the  $\pi^*$  orbital and g) for the  $\sigma^*$  orbital for transitions localized near 4.7 eV. Laser photodissociation spectroscopy results are reproduced from Matthews *et al.*, *J. Chem. Phys.* **148**, 084304 (2018), with the permission of AIP Publishing. One color photoelectron spectra are adapted from Ref. 24 with permission from the Royal Society of Chemistry.

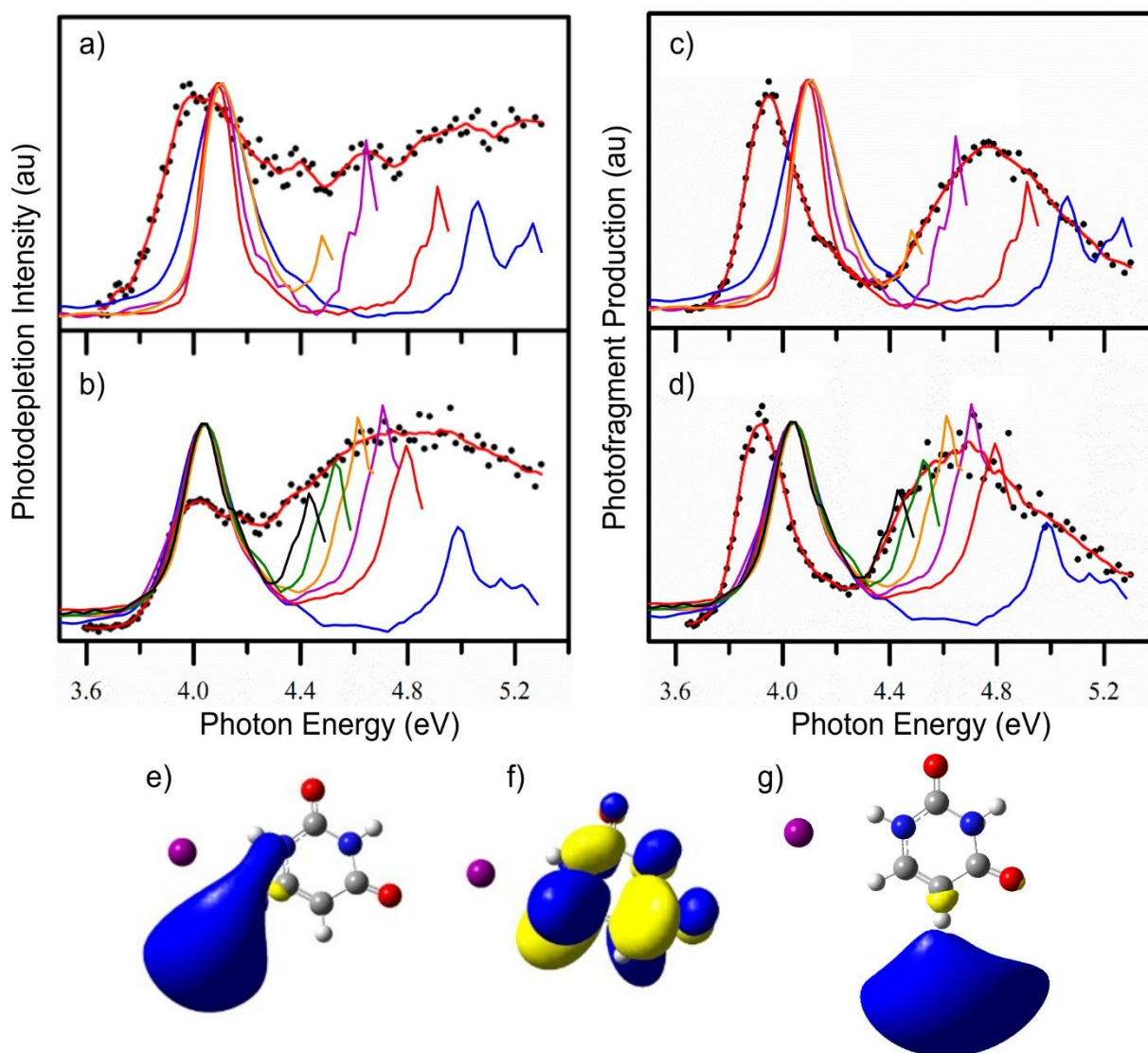




Figure 9. Diagram of the approximate energies and ranges for the various excited states of  $I^- \cdot U$  accessed in this work, as well as the proposed pathways resulting from near-VDE photoexcitation (green photon, black arrows) and higher energy photoexcitation (purple photon, blue arrows). DBS and VBS denote the DB and VB states, respectively.

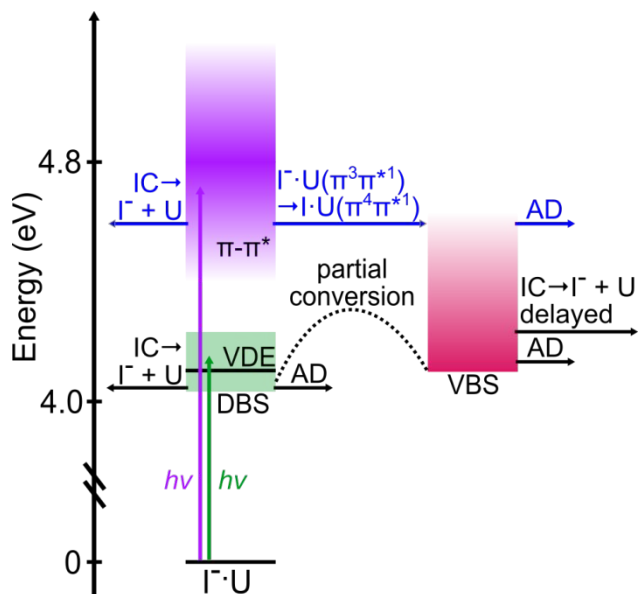


Figure 10. Calculated potential energy surfaces corresponding to a DB to VB anion transition within the a) A9 and b) A3 tautomers of adenine and c) between the A9 DB anion to form the A3 VB anion. The linear scaling factor  $s$  refers to the linear interpolated geometries between the equilibrium DB anion ( $s=0$ ) and the equilibrium VB anion ( $s=1$ ). Calculated at the CAM-B3LYP/6-311++G(2d,p) level of theory, see original work for additional computational details. Reproduced from Stephansen *et al.*, J. Chem. Phys. **143**, 104308 (2015), with the permission of AIP Publishing.

